small methods
www.small-methods.com

Recent Advances in Low-Dimensional Nanomaterials for Photodetectors

Jaehyun Kim, Junho Lee, Jong-Min Lee, Antonio Facchetti, Tobin J. Marks, and Sung Kyu Park**

New emerging low-dimensional such as 0D, 1D, and 2D nanomaterials have attracted tremendous research interests in various fields of state-of-the-art electronics, optoelectronics, and photonic applications due to their unique structural features and associated electronic, mechanical, and optical properties as well as high-throughput fabrication for large-area and low-cost production and integration. Particularly, photodetectors which transform light to electrical signals are one of the key components in modern optical communication and developed imaging technologies for whole application spectrum in the daily lives, including X-rays and ultraviolet biomedical imaging, visible light camera, and infrared night vision and spectroscopy. Today, diverse photodetector technologies are growing in terms of functionality and performance beyond the conventional silicon semiconductor, and low-dimensional nanomaterials have been demonstrated as promising potential platforms. In this review, the current states of progress on the development of these nanomaterials and their applications in the field of photodetectors are summarized. From the elemental combination for material design and lattice structure to the essential investigations of hybrid device architectures, various devices and recent developments including wearable photodetectors and neuromorphic applications are fully introduced. Finally, the future perspectives and challenges of the low-dimensional nanomaterials based photodetectors are also discussed.

1. Introduction

Over the past several decades, the development of various novel photodetectors (PDs) has been tremendously explored for wide fields of emerging optoelectronic technologies and photonic applications throughout our daily lives such as optical communications,[1–3] remote control devices,[4–6] smart image sensing,[7–9] and bio-photonic electronics.[10,11] Recently, PDs, which can convert light signals into electrical signals, are attracting considerable attention due to the increasing demands for accurate detection of various wavelength of light ranging from X-rays (0.03–3 nm),[12–14] ultraviolet (UV, 0.01–0.4 μm),[15–17] visible (0.4–0.75 μm),[18–21] to infrared (0.75 μm–1 mm)[22–24] as well as astronomical detection[25–27] to offer great potential in revolutionary improvements of sensory device performances with multiplexed functionalities. In particular, silicon technologies such as complementary metal-oxide-semiconductors (CMOS)-compatible epitaxial semiconductors have led to the development of commercial cost-effective PDs with the large area and scalable optoelectronic systems.[24,28,29] However, their limited sensing and actuation properties of the silicon semiconductors have been a critical obstacle to unlock the vast potential for realization of high-performance photonic devices and state-of-the-art wearable PDs due to the mechanically rigid and fragile characteristics. Therefore, various promising and prospective photonic materials have been persistently developed to overcome conventional technologies. In particular, new classes of low-dimensional nanomaterials in nonconventional device architectures have been extensively researched due to their outstanding electrical and photonic characteristics such as high sensitivity, excellent carrier mobility, great chemical and thermal stability, and physical properties. In addition, high-throughput production capabilities of low-dimensional nanomaterials enable to significantly decrease production costs and increase fabrication throughput for large-area integration.[30–33]

Significant advances in producing various low-dimensional such as 0D,[34,35] 1D,[36] and 2D[37,38] nanomaterials have been explored to improve the optoelectronic performances and functionalities of PDs. In nanometer-scale materials, electronic performances and functionalities are strongly dependent on their atomic structural conformation and interface interactions with other materials.[39] In terms of dimensions, 2D layered materials confine the movement of the carriers in the one spatial

J. Kim, A. Facchetti, T. J. Marks
Department of Chemistry and Materials Research Center
Northwestern University
Evanston, IL 60208, USA
E-mail: t-marks@northwestern.edu
J. Lee, J.-M. Lee, S. K. Park
Displays and Devices Research Lab. School of Electrical and Electronics Engineering
Chung-Ang University
Seoul 06974, South Korea
E-mail: skpark@cau.ac.kr
The ORCID identification number(s) for the author(s) of this article can be found under https://doi.org/10.1002/smtd.202300246

DOI: 10.1002/smtd.202300246

dimension within the nanoscale.[40] Covalent bonds are formed by the in-plane atoms while the 2D layers are bonded by van der Waals (vdW) forces, resulting in atomic level ultrathin thickness. The 2D materials such as graphene,[41–43] transition metal dichalcogenides (TMDCs),[44–51] perovskite,[52–55] and black phosphorus (BP)[56–59] can be fabricated by simple solution-process methods compared to conventional epitaxial semiconductors, exhibiting unique photonic properties such as high optical transparency and great absorption in broadband wavelength. Meanwhile 1D nanostructure materials including nanowires (NWs),[60,61] nanorods (NRs),[62,63] and nanotubes (NTs)[63,64] with 1D limited nanoscale occupy additional 2D confined spatial dimension within the nanoscale, leading to abundant novel phenomena and unique properties. In addition, high surface-to-volume ratio and small diameter make them specifically attractive for potential optoelectronic applications. 0D nanostructured materials such as nanoparticles (NPs)[65] and quantum dots (QDs)[66–68] confine the excitons within all three spatial dimensions. Further, the 0D materials exhibit quantum confinement effect with smaller particle size than the de Broglie wavelength, leading to increase of density of states by tuning energy states with the particle size and shape.[69] As a result, they show unique and excellent photosensitive behaviors with 3D tunability, which make them possible to realize more compact and multifunctional PD systems by reduction of device size and increase of sensor resolution. Furthermore, hybrid implementation of combining multiple nanomaterials enables to control of fundamental drawbacks of single material-based PDs. Thus, a hybridized synergic combination of heterostructure optoelectronics and PD devices have been demonstrated to enlarge applications and improve the photonic performance and functionalities.[70–72]

From the unique structure and optical properties of low-dimensional nanomaterials, various PD applications such as photodiodes and phototransistors can be designed.[73] For example, photodiodes have been developed for typical two-terminal PD devices to transport photoexited carriers toward the cathode and anode with the advantages of simple fabrication, high resolution, and fast response time. In addition, as the three-terminal PD devices, phototransistors associate the functionality of thin-film transistors where the conductivity can be controlled by the gate field, leading to high photosensitivity and photoconductive gain. Furthermore, high-quality low-dimensional nanomaterials have been proposed to offer remarkable capabilities of new prospect of bioinspired wearable sensor electronics for the conformal PD applications due to their mechanically flexible appearance with great optoelectronic properties.[74] Therefore, the integration of low-dimensional nanomaterials with printable and flexible platforms opens a facile route to realize state-of-the-art electronic and optoelectronic applications.

In this review, we first briefly introduce some of the low-dimensional nanomaterial-based PDs that have been primarily researched and provide device applications such as photodiode, photoconductors, and phototransistors. Subsequently, we focus on imaging and neuromorphic devices as well as flexible/wearable PD applications. Finally, brief summary and possible challenges/opportunities are presented related to the fields of these PDs and future development.

2. Low-Dimensional Nanomaterial-Based PDs

2.1. 2D Nanomaterials

2.1.1. Graphene

Graphene, single atom layer of sp^2 bonded carbon arranged in honeycomb lattices or one single layer of graphite, has provided a new perspective in optoelectronics since its first discovery in 2004 by Geim et al.[58] Graphene exhibits various unique electron transport properties in 2D atomic crystals such as linear energy–momentum relationship, zero bandgap, and anomalous quantum Hall effect, demonstrating extraordinary electronic, mechanical, thermal, and optoelectronic characteristics such as ultrahigh electron mobility, optical transparency, mechanical strength, and thermal conductivity.[75] For the preparation of graphene, two main methods such as top-down and bottom-up synthesis have been widely explored. The top-down synthesis of graphene involves mechanical exfoliation, liquid-phase exfoliation, electrochemical exfoliation, and chemical oxidation reduction.[76–79] Xia et al. have reported ultrahigh-bandwidth PDs based on single and few-layer graphenes which are prepared by mechanical exfoliation of graphite.[80] Internal field near the interfaces between electrode and graphene produces ultrafast photocurrent generation and transport in graphene, leading to extremely high bandwidth (potentially >500 GHz), zero dark current operation, and good internal quantum efficiency (6–16%). One strategy to improving performance is integrating a graphene onto a silicon-on-insulator (SOI) bus waveguide. Gan et al. prepared waveguide-integrated graphene PDs using a metal-doped graphene junction which separates the photoexcited carriers.[81] The interaction between graphene silicon waveguide optical mode leads to high photoresponsivity exceeding 0.1 A W^{-1} in the response range from 1450 to 1590 nm and high response rate exceeding 20 GHz. In addition, Zhang et al. demonstrated monolayer graphene-based PDs through band structure engineering for creating a bandgap in graphene and electron trapping centers to increase photoresponsivity.[82] As a result, pure graphene PDs showed a higher photoresponsivity of 8.61 A W^{-1} and broad photoresponse from the visible (532 nm) to the mid-infrared (10 μm).

Meanwhile, the bottom-up synthesis includes chemical vapor deposition (CVD), epitaxial growth, thermal pyrolysis, chemical synthesis, and laser-assisted synthesis.[42] Among them, CVD processing is particularly one of the most common methods for commercial products of graphene synthesis due to simple and low-cost way to guarantee large and scalable quantities.[78] A key strategy to increase the performance of graphene-based PDs was using a photogating mechanism. Jiang et al. introduced periodic silicon grating into the monolayer graphene to enhance interface potential, achieving 240 A W^{-1} and 3.4×10^{12} Jones of photoresponsivity and detectivity, respectively, in the infrared band (1.55 μm) for graphene-based SOI PDs.[83] Photogenerated carriers are separated efficiently, and recombination of charges is hindered in the graphene channel, leading to an enhanced photogating effect. Sasssi et al. presented an uncooled, mid-infrared PDs that use a floating metallic structure to concentrate pyroelectric charge on a graphene top-gate capacitor, resulting in high gain and temperature coefficient of resistance up to 900% K^{-1}, with the ability

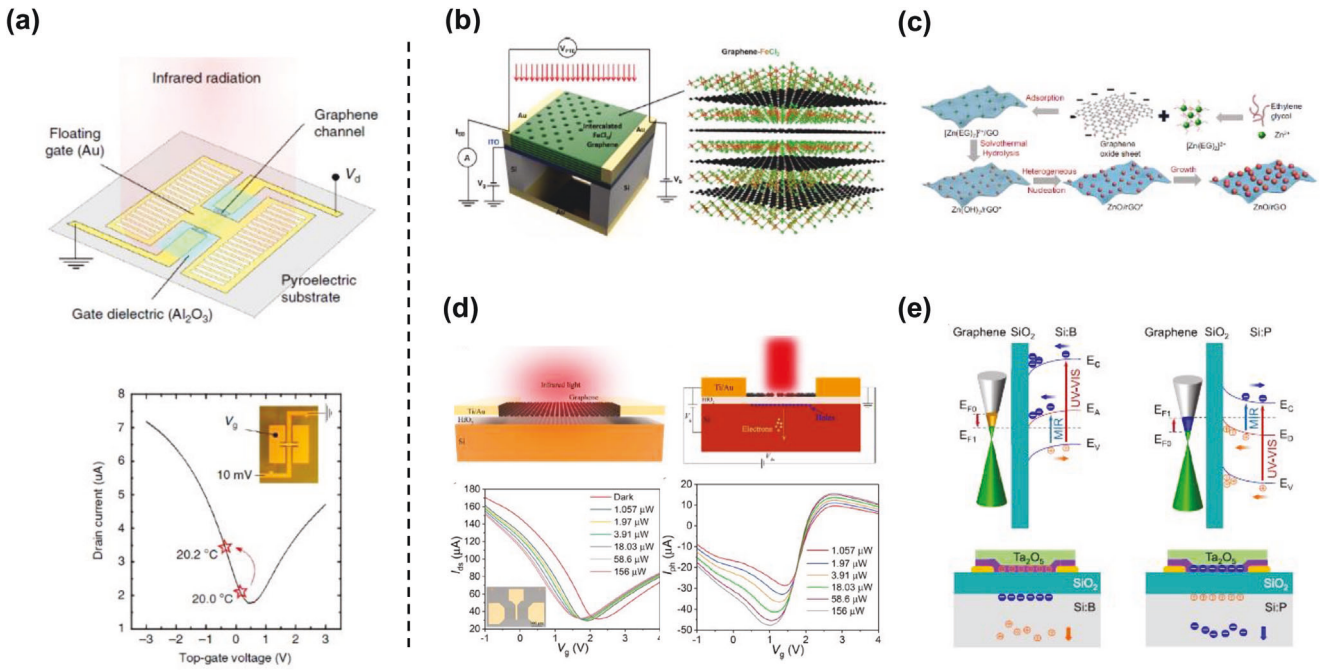

Figure 1. a) Scheme of an individual device, where the conductance of a single-layer graphene channel is modulated by the pyroelectric substrate and by a floating gate. Reproduced with permission.[84] Copyright 2017, Nature Publishing Group. b) Schematic showing our proposed ultrafast near-infrared-short-wave-length infrared photodetector based on suspended monolayer graphene intercalated with $FeCl_3$ placed on top of a cavity, which can be tuned by means of a gate voltage applied to the ITO layer. Reproduced with permission.[85] Copyright 2022, American Chemical Society. c) Schematic illustration of the growth mechanism of ultrafine ZnO/rGO nanocomposites. The whole process is an adsorption-nucleation-growth process. Reproduced with permission.[86] Copyright 2022, Nature Publishing Group. d) Schematic view of the graphene/HfO_2/Si photodetector with a pair of Ti/Au source-drain electrodes. Reproduced with permission.[87] Copyright 2021, American Chemical Society. e) Scheme of the graphene-based mid-infrared photodetectors. Reproduced with permission.[88] Copyright 2022, American Chemical Society.

to resolve temperature variations down to 15 mK (**Figure 1**a).[84] Different strategies were explored to enhance absorbance and extend absorption wavelength of graphene. Shabbir et al. recently proposed nanopatterned multilayer graphene based PDs for realizing ultrafast photodetection and high photoresponsivity in the infrared regimes (Figure 1b).[85] The localized surface plasmons on the graphene along with an optical cavity enable to increase the absorbance from around 2% to nearly 100% for nanopatterned multilayer graphene with $FeCl_3$, achieving high photoresponsivity of 6.15×10^3 V W^{-1}, detectivity of 2.3×10^9 Jones, and ultrafast response time of about 100 ns in the infrared regimes between 1.3 and 3 μm. Zhang et al. synthesized ultrafine metal oxide/reduced graphene oxide (rGO) nanocomposites through a heterogeneous nucleation and diffusion-controlled growth process to achieve high solute rejections and water flux in dye nanofiltration (Figure 1c).[86]

Huang et al. used CVD-grown graphene based on copper foil for broadband PDs in the range from visible (473 nm) to mid-infrared (2.7 μm).[87] An interfacial gating effect was examined in the graphene-based PDs onto silicon substrate with HfO_2 due to the high interface state density at the interface between silicon and HfO_2, leading to high photoresponsivity as high as 45.8 A W^{-1} (Figure 1d). The anchored ultrafine nanoparticles inhibited wrinkling of the rGO nanosheet and increased both vertical interlayer spacing and lateral tortuous paths of the rGO membranes, resulting in a high water permeability of 225 L m^{-2} h^{-1} bar^{-1} and selectivity up to 98% in the size-exclusion separation of methyl blue. Another route for realizing high detectivity and fast photoresponse of graphene-based PDs is by integration heterojunction hybrid devices. Peng et al. demonstrated graphene and 2D tellurium heterojunction hybrid PDs with high detectivity of 1.04×10^9 Jones and fast response time of 28 μs under short-wave infrared irradiation (2 μm).[89] With the built-in electric field in the band-matched heterojunction, photogenerated electron-hole pairs are separated efficiently and photocurrent is generated. Chen et al. reported graphene PDs using organic heterostructure composed of perylene-3,4,9,10-tetracarboxylic dianhydride (PTCDA) and pentacene as the light-absorbing layer.[90] The heterostructure enables to improve electron–hole pair dissociation efficiency due to interfacial built-in field, exhibiting very high photoresponsivity of 10^5 A W^{-1}, fast response time down to 30 μs, and high quantum efficiency up to 64%, which are significantly improved compared with each individual material. In addition, Han et al. realized broadband PDs based on graphene and C60/pentacene heterojunction with high photoresponsivity of 9.2×10^3 and 1.8×10^3 A W^{-1} in the visible and near-infrared regime, respectively, fast response time down to 300 μs, and high external quantum efficiency up to 11.5%.[91] They first demonstrated bi-directional photoresponse characteristics of PDs at different wavelengths, using unique band alignment which enables to vary charge transfer direction. Graphene can also cover the use in imaging devices by integrating with charge-coupled devices

(CCD) and CMOS technology. Liu et al. investigated graphene charge-injection PDs which are combined with the charge integration properties of CCD and the pixel structure of CMOS.[92] These PDs consist of sandwiched structure between graphene and deep-depletion silicon well for both direct field-effect readout and broadband charge injection, offering high sensitivity above 0.1 and 6×10^4 A W^{-1} in the infrared and visible regime, respectively, and high speed less than 1 μs as well as broadband imaging from UV (375 nm) to mid-infrared (3.8 μm). This may make new imaging devices for possible various fields of photodetection applications. Ho et al. have also demonstrated the operation of pure graphene PDs in a broadband range from deep UV to mid-infrared regions by utilizing photoionization and over bandgap excitation in highly doped Si:B and Si:P substrates, which can pave the way for the development of mid-infrared PDs (Figure 1e).[88]

2.1.2. TMDCs

TMDCs are composed of a combination of two elements with the formula MX_2, where M is a transition metal element from group IVB such as titanium (Ti), zirconium (Zr), or hafnium (Hf), group VB such as vanadium (V), niobium (Nb), or tantalum (Ta), or group VIB such as molybdenum (Mo) or tungsten (W) and X is a chalcogen such as sulfur (S), selenium (Se), or tellurium (Te).[44] Generally, TMDC materials form layered sandwich structures of X-M-X, with a hexagonal lattice which consists of two layers of chalcogen atoms separated by a layer of transition metal atoms. And their adjacent layers are combined by week vdW forces to form the bulk crystal, while the in-plane atoms are bonded by strong covalent bond, thus bulk TMDCs can be easily exfoliated into single- or few-layer 2D nanosheets. Several 2D semiconducting TMDC materials exhibit layer-dependent optical properties, for example, MoS_2 transforms the bandgap from an indirect state of 1.3 eV in their multilayer forms to a direct state of 1.8 eV in the monolayer.[93–95] The direct bandgap of monolayer TMDCs results in efficient photoluminescence, which opens the possibility for developing optoelectronics. In addition, there are many interesting photonic properties in layer-dependent TMDCs, thus, the 2D form of TMDCs is being considered as one of the most unique and promising materials for electronic and optoelectronic devices.[96]

In general, there are two synthesis methods for producing 2D TMDCs, such as the top-down and the bottom-up approaches.[97] Top-down synthesis strategies include mechanical cleavage and liquid exfoliation.[50] Atomically thin mono- and few- layers of 2D TMDC flakes can be peeled from bulk materials by micromechanical exfoliation using adhesive tape due to the weak vdW coupling between layers. For obtaining large-scale of 2D TMDCs with high yield, liquid phase exfoliation methods have been demonstrated as promising approaches with the use of liquids which act as solvent or chemical. Such methods can be subdivided into two routes such as direct exfoliation using ultrasonication or shearing and chemical exfoliation using chemical and electro-chemical intercalation.[98] 2D monolayer TMDCs can be exfoliated via molecules insertion within the interlayer of the bulk crystal by surface energy difference. The main advantage of liquid exfoliation is that it produces additional applications such as solution-based flexible and large-area printable electronics and optoelectronics, while extrinsic defects during the exfoliation process can be introduced, thus it may require additional post treatment to improve the quality of the 2D TMDC structures.

Bottom-up synthesis approaches via vapor phase deposition have been also attempted to produce large-area and uniform 2D TMDCs with scalable and controllable thickness.[99] As previously prepared for graphene, the development of bottom-up synthesis includes via CVD on metal substrates such as sulfurization/selenization process using metal/metal oxide film or vaporization of transition metal oxides with chalcogen precursors, or by wet chemical routes such as hydrothermal or solvothermal methods.[100] Typically, the bottom-up synthesis strategies exhibit various advantages compared with top-down approach methods, such as inexpensive instruments, versatile and relatively high-quality resulting materials, and larger size of continuous film. Yu et al. synthesized mono- or few-layer MoS_2 films via CVD approach over an area of centimeters with high uniformity as shown in **Figure 2**a.[101] In particular, the MoS_2 layer numbers can be precisely controlled from mono to several layers and the films exhibited good polycrystalline quality. Zhang et al. realized CVD-grown high-quality and uniform 2D MoS_2 flakes via Tin (Sn) atoms doping into MoS_2 crystals for improving optical characteristics (Figure 2b).[102] As a result, Sn-doped MoS_2 PDs showed high photoresponsivity up to 29 A W^{-1}, external quantum efficiency (EQE) of 7.8×10^3%, and detectivity of 10^{11} Jones at 470 nm of wavelength.

One advanced research direction for enhancing electronic and optical functionality is the stacking of various different 2D TMDC materials for vertical heterostructures and hybrid devices.[98,103,104] Li et al. prepared 2D heterostructure via the integration of MoS_2 and graphitic carbon nitride nanosheets using a simple impregnation and calcination method.[105] The 2D heterojunction formation between the MoS_2 and graphitic carbon nitride encourages charge transfer and photogenerated electron-hole pairs separation efficiency, leading to photocatalytic activity and stability enhancement under visible light region. Chen et al. have synthesized a series of 2D TMDC heterostructures, including a MoS_2–WS_2 vertical heterostructure, $Mo_{1-x}W_xS_2$ alloy, and WS_2 bilayer, via ambient pressure CVD system under various growth temperature.[106] The vertical and lateral 2D TMDC heterostructures were constructed with large-scale triangular flakes and four-point star-like flakes for WS_2–MoS_2–WS_2 lateral structures and strong interlayer excitonic interactions were observed between MoS_2 and WS_2 and between WS_2 and $Mo_{1-x}W_xS_2$. Sahoo et al. fabricated bilayer lateral 2D TMDC heterostructures based on MoS_2–WS_2 and $MoSe_2$–WSe_2 monodomains.[107] A scalable and sequential lateral CVD method was used to make lateral heterostructures, and they showed clear photovoltaic response with room-temperature electroluminescence. Najafidehaghani et al. reported electronic and optoelectronic applications based on $MoSe_2$-WSe_2 lateral 2D TMDC heterostructures using a scalable one-pot CVD process (Figure 2c).[108] Particularly, PDs based on large-area monolayer formation of heterostructure exhibited high photoresponsivity of 18 mA W^{-1}, detectivity of 10^9 Jones, and fast response time of about 0.15 s in the visible light region (520 nm). Wang et al. devel-

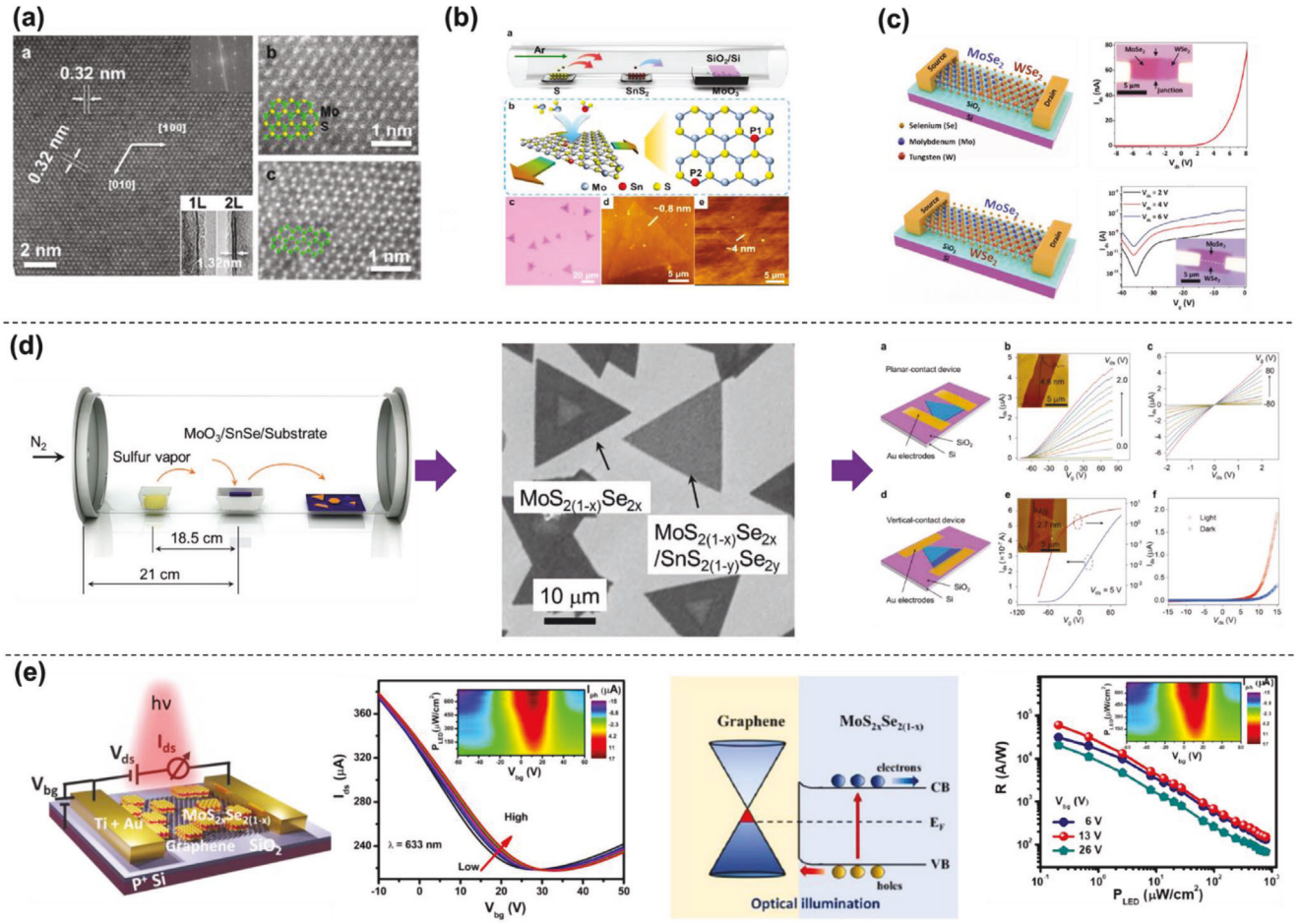

Figure 2. a) Characterization of the crystal structure of synthesized MoS_2 monolayer and bilayer films. Reproduced with permission.[101] Copyright 2013, Nature Publishing Group. b) Schematic representation of the CVD setup for Sn doped MoS_2 and atomic structure of the as-grown products and the AFM surface morphologies. Reproduced with permission.[102] Copyright 2021, American Chemical Society. c) Electronic and optoelectronic characterization of p–n junction devices fabricated using the $MoSe_2$–WSe_2 lateral heterojunctions. Reproduced with permission.[108] Copyright 2021, Wiley-VCH. d) Schematic illustrating the single-step chemical vapor synthesis of alloy-based vertical heterostructures and typical scanning electron microscopy images of the as-grown samples. Schematic of the planar and vertical-contact heterostructure device and the I_D–V_G transfer characteristics of the planar and vertical-contact device measured at various bias voltages V_D. The inset shows an AFM image of the planar-contact device. Reproduced with permission.[109] Copyright 2021, Wiley-VCH. e) Graphene–$MoS_{2x}Se_{2(1-x)}$ alloy based phototransistors for high-performance and broad-band photodetection. Reproduced with permission.[111] Copyright 2022, American Chemical Society.

oped 2D vertical heterostructures of $MoS_{2(1-x)}Se_{2x}/SnS_{2(1-y)}Se_{2y}$ grown by single-step CVD method of alloy-to-alloy synthesis.[109] With the epitaxial interfaces and enhanced electronic transport properties, PDs based on $SnS_{1.7}Se_{0.3}/MoS_{0.8}Se_{1.2}$ 2D vertical heterostructures showed high rectification ratio of 173. This approach can broaden material designs and combinations of multilayered 2D TMDC heterostructures and offer innovative and novel method for optimizing PD applications. The schematic of devices and the characteristics were shown in Figure 2d. Recently, Zeng et al. developed a $PbS/MoS_2/WSe_2$ heterostructure photodiode to enhance the photovoltaic response, achieving a broadband photovoltaic response with a high responsivity of 0.76 A W^{-1}, and a specific detectivity of 5.15×10^{11} Jones while not sacrificing response speed, using a scheme that provides opportunities for high-performance 2D vdW optoelectronic devices.[110] Mukherjee et al. reported alloy engineering in 2D TMDCs led to the development of hybrid phototransistors, including a graphene-MoSSe device with high photoresponsivity, low noise equivalent power, and excellent gate tunability, demonstrating the scalability and potential for wafer-scale production of high-performance optoelectronic devices (Figure 2e).[111] Dodda et al. used a monolayer MoS_2 based phototransistor technology that offers low energy consumption, small device size, and high dynamic range sensing, as well as fast reset and de-noising capabilities. This technology is considered to be beneficial for edge devices in the Internet of Things (IoT) industry.[112]

2.1.3. Perovskites

Perovskites generally have a crystallographic structure in the form of ABX_3, where A is a monovalent inorganic or organic cation such as cesium (Cs^+), methylammonium (MA, $CH_3NH_3^+$), or formamidinium (FA, $CH(NH_2)_2^+$), B is a bivalent

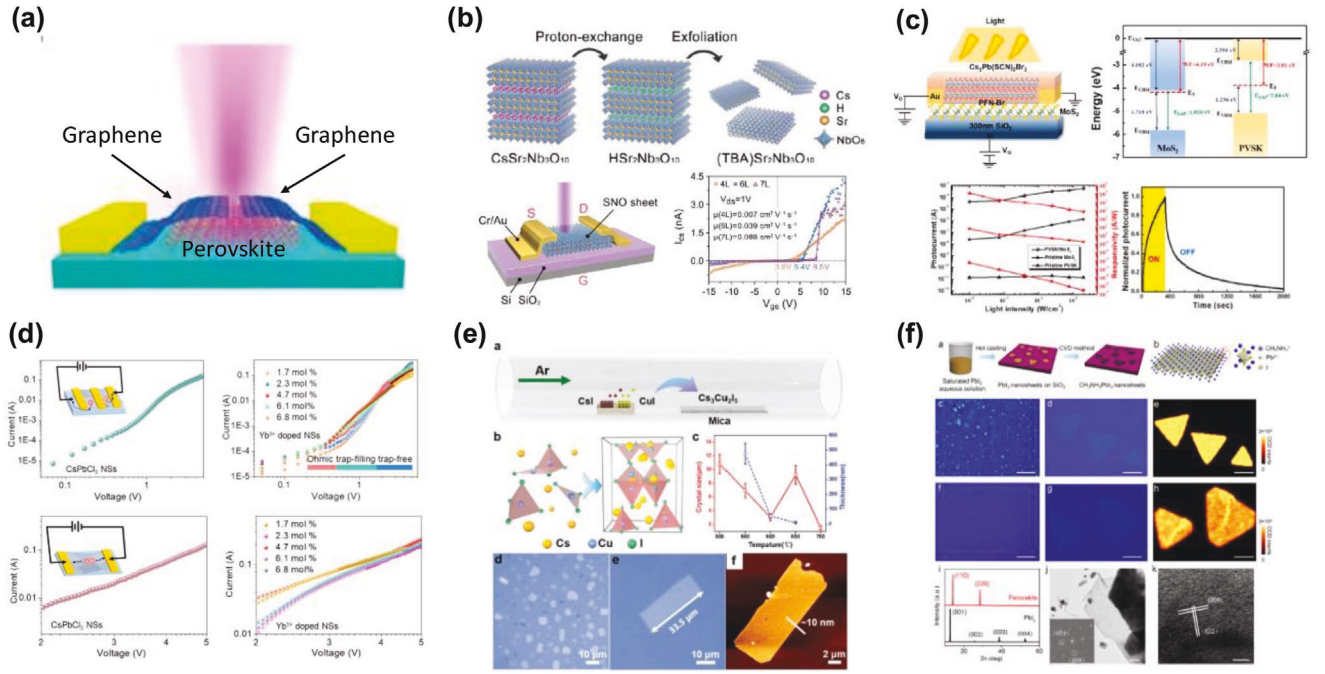

Figure 3. a) Schematics of the graphene contacted 2D perovskite photodetector. Reproduced with permission.[117] Copyright 2016, American Chemical Society. b) The schematic illustration of the preparation process of $Sr_2Nb_3O_{10}$ nanosheets via proton-exchange and exfoliation processes from bulk precursor $CsSr_2Nb_3O_{10}$ and the transfer characteristics of $Sr_2Nb_3O_{10}$ transistors with various thicknesses in dark condition. Reproduced with permission.[121] Copyright 2020, Wiley-VCH. c) Device structure of the fabricated $Cs_2Pb(SCN)_2Br_2/MoS_2$ hybrid photodetector and its band structure and comparison of photocurrent and responsivity of the photodetectors. Reproduced with permission.[123] Copyright 2021, Elsevier. d) *J–V* characteristics of photodetectors with ITO/$CsPbCl_3$ nanosheets/Au. Reproduced with permission.[124] Copyright 2022, Elsevier. e) Schematic diagram of the CVD setup for the synthesis of $Cs_3Cu_2I_5$ nanosheets and the atomic structure of $Cs_3Cu_2I_5$ crystal. And thickness and size distributions of $Cs_3Cu_2I_5$ crystals versus growth temperatures. Optical image of as-grown $Cs_3Cu_2I_5$ crystals on a mica substrate and an $Cs_3Cu_2I_5$ nanosheet as large as 33.5 μm. And the AFM image and height measurement over an exemplary $Cs_3Cu_2I_5$ flake. Reproduced with permission.[125] Copyright 2022, Wiley-VCH. f) Schematic illustration of solution process to fabricate 2D PbI_2 nanosheets and vapor-phase conversion process to transfer PbI_2 into 2D $CH_3NH_3PbI_3$ perovskite nanosheets. And corresponding optical image and TEM image. Reproduced with permission.[126] Copyright 2022, American Chemical Society.

metal cation such as lead (Pb^{2+}), Sn^{2+}, or germanium (Ge^{2+}), and X is a halide anion such as chloride (Cl^-), bromide (Br^-), or iodide (I^-). In general, 2D perovskites are obtained by cutting along the <100>, <110>, and <111> crystallographic planes of the 3D perovskite structure, which results in three different <100>-, <110>-, and <111>-oriented 2D perovskites, respectively.[55] Particularly, the <100>-oriented 2D perovskites are mostly used, which are further categorized into three types such as the Ruddlesden-Popper (RP), the Dion-Jacobson (DJ), and alternating cations in the interlayer (ACI) phase with distinct capping cation within the inorganic layers.[113,114] The RP and DJ phase adopt chemical formulas of $A'_2A_{n-1}B_nX_{3n+1}$ and $A''A_{n-1}B_nX_{3n+1}$, respectively, where A′ is a monovalent cation such as phenylethylammonium (PEA^+) and butylammonium (BA^+) and A″ is a divalent cation such as 3-(aminomethyl)piperidinium ($3AMP^{2+}$) and 1,4-butane diammonium (BDA^{2+}).[115] The n is referred to as the number of inorganic layers, which is generally given based on the stoichiometry of precursor. In addition, the 2D perovskite structure is determined by the *n* value, where $n = 1$ and $1 < n \leq 5$ for pure 2D and quasi-2D perovskite structure, respectively. In particular, multiple quantum wells are achieved when n is high value due to different formation energy, thus preparing phase-pure 2D perovskite films with high-*n* value is always challenging.[116]

Tan et al. reported the first PD based on individual 2D $(C_4H_9NH_3)_2PbBr_4$ perovskite crystals, achieving a high responsivity of ≈2100 A W^{-1} and extremely low dark current (≈10^{-10} A) with a design of interdigital graphene electrodes as shown in **Figure 3**a.[117] Also, in terms of the structural and morphological properties, 2D perovskites can be synthesized into all-inorganic or organic-inorganic hybrid forms.[118–120] Li et al. prepared 1.8 nm of 2D all-inorganic perovskite $Sr_2Nb_3O_{10}$ which is synthesized via liquid exfoliation process and two-step high-temperature solid-state reaction (Figure 3b).[121] The 2D perovskite $Sr_2Nb_3O_{10}$ nanosheets based UV PDs exhibited high detecting performance such as photoresponsivity of 1.2×10^3 A W^{-1}, detectivity of 1.4×10^{14} Jones, EQE of 5.6×10^5%, and fast response time of 0.4 ms in the wavelength of 270 nm. Further, carrier transport properties and corresponding optoelectronic performances were controlled by bias conditions and thickness of perovskite nanosheets. Wang et al. have prepared all-inorganic pure and homogeneously distributed 2D perovskite $CsPb_2Br_5$ nanosheets via environmentally friendly chemical precipitation methods in water and ethanol assistant solvent to provide the supersaturation and boost nucleation of the nanosheets.[122] Specifically, low substrate temperature was used for optimizing the morphology of nanosheets with less stacking. Thus, PDs based on

2D perovskite $CsPb_2Br_5$ nanosheets demonstrated high photoresponsivity of 25.9 mA W^{-1}, detectivity of 1.37×10^{10} Jones, and fast response time of less than 50 ms. Chu et al. reported a unique 2D all-inorganic perovskite such as $Cs_2Pb(SCN)_2Br_2$ which is prepared by partially substituting the halide anion with an asymmetric pseudo-halide anion, such as SCN anion (Figure 3c).[123] The 2D $Cs_2Pb(SCN)_2Br_2$ possesses small spacing between perovskite sheets and leads to enhanced charge transport efficiency. As a result, 2D perovskite $Cs_2Pb(SCN)_2Br_2$ based PDs exhibited high photoresponsivity of 1.22×10^5 A W^{-1} and fast photoresponse time of 166 ms. More recently, Sun et al. developed 2D all-inorganic perovskite $CsPbCl_xBr_{3-x}$ nanosheets which are doped with ytterbium ion (Yb^{3+}) using hot-injection method to increase their optical and electrical properties, resulting in high optimal photoluminescence quantum yield of 128% at 985 nm, due to the passivation effect of Yb^{3+} doping and reducing defect density of the 2D perovskite (Figure 3d).[124] Further, PDs based on Yb^{3+}-doped $CsPbCl_xBr_{3-x}$ nanosheets exhibited high photoresponsivity about 2 A W^{-1} and detectivity larger than 10^{12} Jones at 440 nm. Lv et al. prepared 2D all-inorganic perovskite $Cs_3Cu_2I_5$ nanosheets, which are epitaxially grown with high phase quality less than 10 nm of thickness, by moderate-temperature CVD method.[125] Figure 3e shows $Cs_3Cu_2I_5$ nanosheets with strong blue emission, which is originated from large Stokes shift and long photoluminescence decay time. They also found that UV PDs based on $Cs_3Cu_2I_5$ perovskites reveal a high photoresponsivity of 3.78 A W^{-1}, and fast response time less than 200 ms at 270 nm region.

Hybrid organic–inorganic 2D perovskite materials have been also extensively demonstrated. Liu et al. synthesized 1.3 nm of 2D hybrid $CH_3NH_3PbI_3$ perovskites via a combined solution process and CVD method (Figure 3f).[126] The thickness and composition-dependent tunable photoluminescence was exhibited in triangle and hexagonal shapes of $CH_3NH_3PbI_3$ perovskites, and PDs based on 2D hybrid perovskites showed high photoresponsivity larger than 10 A W^{-1} in the visible region. Ma et al. developed novel form of 2D hybrid organic−inorganic lead halide perovskites such as chiral $(MBA)_2PbI_4$ where MBA is $C_6H_5C_2H_4NH_3$ which are synthesized with a needle shape by incorporating the chiral molecules.[127] The chiral 2D perovskites exhibit a maximum circularly polarized photoluminescence of 17.6%. Lin et al. used hexane and chlorobenzene orthogonal solvents for single-crystalline perovskites 2D hybrid perovskite such as $(MBA)_2PbI_4$.[128] With a less than 10 nm thick single-crystal 2D perovskite nanosheet, nanoscale PDs showed high responsivity of 5.4 mA W^{-1} and detectivity larger than 10^{13} Jones. Furthermore, Yang et al. demonstrated hybrid heterostructures based on 2D perovskites for enhancing the optoelectronic performance of PDs.[129] They designed few nanometer thick perovskite-based vertical semiconductor heterostructure with monolayer TMDC such as WS_2, which leads to highly efficient charge carrier transport. Thus PDs based on this heterostructure represented high photoresponsivity about 1.1×10^4 A W^{-1} and fast response time less than 70 µs. Hossain et al. reported that solution-processed 2D perovskites such as $(CH_3(CH_2)_3NH_3)_2(CH_3NH_3)_{n-1}Pb_nI_{3n+1}$ ($n = 4$) via inkjet-printing using magnetic stirring at room temperature.[130] All inkjet-printed 2D perovskite-based PDs confirmed high photoresponsivity of 0.53 A W^{-1} and detectivity larger than 10^{13} Jones. The solution processed 2D perovskites may produce significant possibility of low-cost and large-scale production for future flexible electronics and optoelectronics.

2.1.4. BP

Since the rediscovery of 2D BP in 2014,[131] it has been considered as one of the most fascinating materials for the applications of optoelectronics due to its desirable intrinsic properties such as direct and tunable bandgap which depends on the number of layers from about 0.3 eV for bulk to 1.5 eV for the monolayered structure.[132,133] In addition, it possesses excellent carrier mobility up to 1000 cm^2 V^{-1} s^{-1} at room temperature as well as highly anisotropy-dependent thermal, electrical, optical properties, and mechanically durability.[131,134,135] BP is considered as the most stable phosphorus allotrope under room temperature and pressure with a layered vdW crystal and an orthorhombic structure.[136] Furthermore, BP has distinct and unique crystal structure compared with other 2D materials which form a ridge structure along the zigzag direction and puckered honeycomb structure along the armchair direction and this structural anisotropy can be seen due to the local bonding configurations. Thus, for each single layer of two atomic layers, bond lengths between two nearest atoms (2.224 Å) and between top and bottom atoms (2.244 Å) are not identical and bond angles are not equal (96.34° and 102.09°).[137] Such a unique substantial in-plane anisotropy and hinge-like structural arrangement leads to anisotropic physical properties such as a negative Poisson ratio.

Similar to graphene and other 2D TMDC materials, 2D BP can be produced by top-down approaches such as micromechanical exfoliation method, liquid-phase exfoliation technique, plasma-assisted etching technique, thermal sublimation method, anodic oxidation method, chemical thinning method, and mechanochemical dry process, and by bottom-up approaches such as red phosphorus to BP conversion method, pulsed laser deposition technique, solvothermal process, and epitaxially lateral growth method.[142] In particular, Xu et al. recently developed direct growth of large-scale crystalline 2D BP nanosheet using an Au_3SnP_7-assited gas-phase growth method with an epitaxial nucleation and a lateral growth control on insulating silicon substrates (**Figure 4**a).[138] A few nanometer-thick (5–10 nm) 2D BP nanolayers were successfully synthesized with an extraordinarily lamellar microstructure and they showed orthogonally symmetric structure with high crystallinity, purity, and excellent carrier mobility over 1000 cm^2 V^{-1} s^{-1} at room temperature. The BP also exhibited superior infrared photodetection properties including strengthened infrared absorption and photoluminescence. Liu et al. proposed 2D BP-based hybrid avalanche PDs with silicon for the operation at the wavelengths of 1.55 and 1.95 µm (Figure 4b).[139] They found that hybrid plasmonic waveguide on a thin SOI platform exhibited high responsivity larger than 100 A W^{-1} and excellent 3 dB bandwidth of 1.05 GHz due to the enhanced light absorption and reduced carrier transit time of BP by avalanche multiplication process.

Furthermore, there have been significant efforts to enhance the stability and optoelectronic/physicochemical properties. Thurakkal and Zhang reported chemical functionalization strategy to improve the stability of 2D BP nanosheets using functional

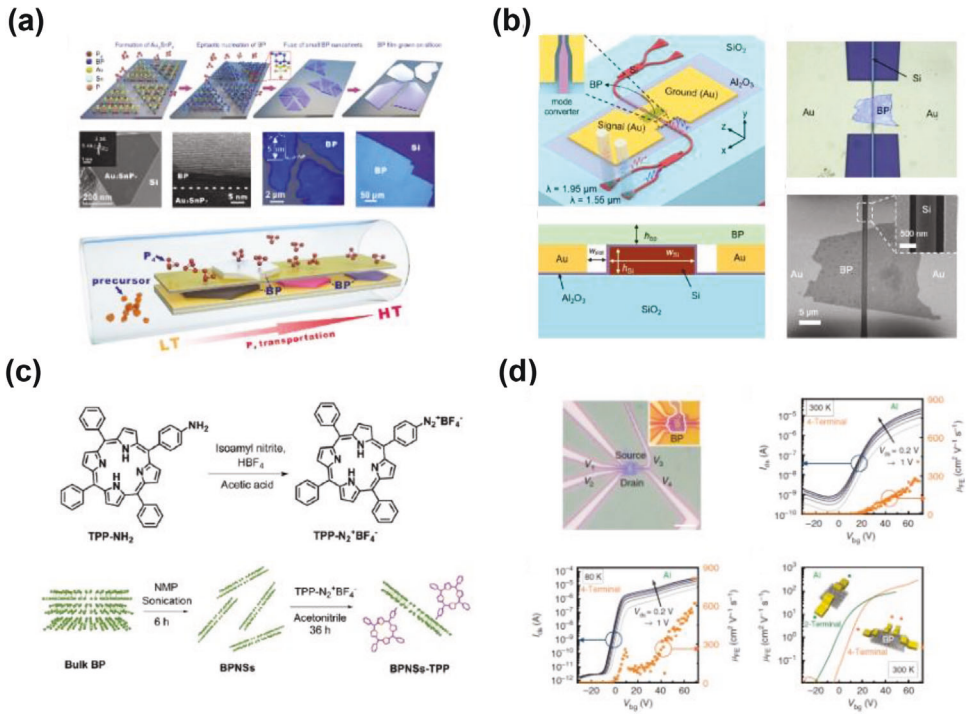

Figure 4. a) Schematic illustration showing the formation of Au_3SnP_7, epitactic nucleation of BP, fuse of small BP nanosheets into large ones on substrate and the SEM image of device. And schematic view of the experimental setup for the BP growth. Specially, red phosphorus was evaporated to P_4 and diffused from low temperature (LT) side toward high temperature (HT) side. Reproduced with permission.[138] Copyright 2020, Nature Publishing Group. b) Structures of the present silicon–BP hybrid plasmonic waveguide PD and corresponding the optical and SEM image. Reproduced with permission.[139] Copyright 2022, American Chemical Society. c) Device structure of the fabricated $Cs_2Pb(SCN)_2Br_2/MoS_2$ hybrid photodetector and its band structure. Reproduced with permission.[140] Copyright 2021, RSC Publication Group. d) High-performance n-type transistors with Al contacts including optical image of the device and the electrical characteristics. Reproduced with permission.[141] Copyright 2015, Nature Publishing Group.

tetraphenyl porphyrin molecules (Figure 4c).[140] The effective functionalization enabled to enhance ambient stability of BP nanosheets such as less than 1% of degradation ratio of optical absorbance variation at 480 nm. Further, the hybrid form of BP nanosheets and porphyrin molecules exhibits electron and energy transport process which is confirmed by decreased lifetime of fluorescence. Kaur et al. demonstrated a straightening method to smoothen and de-wrinkle of 2D BP flakes via electron beam irradiation to improve crystallinity and remove line defects from the lattice.[143] The ironing of BP using electron beam irradiation enabled to control the stress in lattice and the buckling structure of the flake, which can be an important moving forward for controlling 2D atomic nanostructure. Another novel way to enhance optoelectronic properties for PD applications is using hybrid heterostructures. Krishnamurthi et al. explored 2D heterostructures based on vertically stacked BP with MoS_2 nanoflakes for p–n junctions to modulate band alignment and carrier transport efficiency.[144] As a result, PDs based on heterojunction demonstrated high responsivity over 70 A W^{-1}, detectivity of 6.5×10^9 Jones, and EQE larger than 260% at 365 nm wavelength. More recently, Chen et al. constructed 2D BP-based band-aligned vdW heterostructures with 2D Bi_2O_2Se for enhancing charge carrier efficiency and reducing recombination of photogenerated carriers between heterointerfaces.[145] Thus, the hybrid PDs exhibited high responsivity of 1.22 A W^{-1} and quantum efficiency over 80% in the short-wave infrared region. Li et al. suggested vdW heterostructures based on 2D BP and 2D perovskite such as Cs_2SnI_4 for broadening spectrum absorption properties.[146] They found that two types of heterostructures such as Cs-I-BP and Sn-I-BP form a large built-in electric field and have the self-power ability as well as show enhanced absorption coefficients in the UV and infrared regions. At last, Perello et al. developed unipolar n-type black phosphorus transistors with polarity control through contact-metal engineering and flake thickness, exhibiting a leap in n-type performance and exemplifying the logical switching capabilities of black phosphorus.[141] The 13 nm aluminum-contacted flake displays symmetric hole and electron mobilities up to 950 $cm^2\ V^{-1}\ s^{-1}$, while a 3 nm flake displays unipolar n-type switching with on/off ratios greater than 10^7 and electron mobility of 630 $cm^2\ V^{-1}\ s^{-1}$ at 80 K as shown in Figure 4d. These heterostructure approaches broaden optoelectronic properties and multifunctional characteristics of 2D BP-based PD applications.

2.1.5. Other Types of 2D Nanomaterials

Apart from the advancement in traditional graphene and TMDC 2D materials, there have been extensively studied new novel 2D nanomaterials to further enhance performance and functionality for widening optoelectronic applications.[147] 2D soft nanomaterials[148] such as $B_xC_yN_z$ nanosheets including hexag-

onal boron nitride (h-BN), hexagonal boron-carbon-nitrogen (h-BCN), and graphitic carbon nitride (g-CN) nanosheets, 2D polymer including nanographenes and graphene nanoribbons, covalent organic frameworks which are created by periodic covalent linking of monomers, and 2D supramolecular organic nanostructures based on small organic molecules including organic–inorganic hybrid nanosheets have been prepared to open up new possibility for potential applications due to great advantages in light-weight, low-cost, mechanical flexibility, and excellent thermal/optoelectronic performance and stability.[149] In addition, 2D oxides have attracted significant attention due to their advantages such as great air stability with high optoelectronic performance and easy synthetic preparation.[150] With the great advances and efforts, considerable progress has been made on developing 2D oxides such as transition metal oxides including ZnO, MoO_2, VO_2, TiO_2, Cr_2O_3, Fe_2O_3, and WO_3, main-group metal oxides including MgO, SnO, PbO, In_2O_3, Al_2O_3, Ga_2O_3, and Bi_2O_3, and semimetallic oxides including Sb_2O_3, TeO_2, and GeO_2. Alkathiri et al. synthesized 2D palladium sulfate ($PdSO_4$) by oxidation of palladium sulfide (PdS) during the liquid-phase exfoliation process.[151] They found that ultrathin (≈3 nm) 2D $PdSO_4$ planar nanosheets with submicrometer lateral dimensions showed broad visible absorption properties, narrow bandgap, and prolonged exciton lifetime, which is suitable for visible-light-driven optoelectronic applications.

Furthermore, new flatland nanomaterials, commonly known as 2D Xenes such as borophene, arsenene, silicene, germanene, stanene, plumbene, and selenene have recently emerged as a novel platform for biomedical and optoelectronic applications.[152,153] The "X" describes the element and "ene" refers to alkene. 2D Xenes have many fascinating optical and optoelectronic properties such as broadband photoresponse, layer-dependent tunable bandgap, strong nonlinearity, and great stability. MXenes are one of the 2D metal carbides and carbonitrides which can be produced by selective etching of the A phase from a MAX phase of $M_{n+1}AX_n$, where M is a transition metal, A is an A-group element, and X is carbon and/or nitrogen with n is 1, 2, or 3. Hong et al. recently developed centimeter-scale monolayer films (≈1 nm) of 2D MXene such as $MoSi_2N_4$ via CVD method with a Cu/Mo bilayer substrate.[154] By passivating the surface dangling bonds of nonlayered 2D molybdenum nitride, the 2D $MoSi_2N_4$ was successfully grown with excellent ambient stability, high mechanical strength, and great electrical/optical properties. Echols et al. have reported 2D $Ti_3C_2T_z$ MXene-only thin-films via layer-by-layer assembly by functionalization of $Ti_3C_2T_z$ nanosheets.[155] Using positively charged silane-functionalized $Ti_3C_2T_z$ and colloidally stable dispersions, highly electrically conductive $Ti_3C_2T_z$ nanosheets were demonstrated with high optical transparency and capacitance.

Moreover, there have been tremendously efforts to develop new 2D metal chalcogenides beyond the performance of TMDCs. Gao et al. demonstrated ultrasmall 2D PbS nanoplatelets with uniform lateral size and thickness less than 4 nm for 6 layers via facile liquid-phase exfoliation strategy.[156] The 2D PbS nanoplatelets-based PDs exhibited high photoresponsivity of 27.81 mA W^{-1} and detectivity about 4×10^{10} Jones. Guo et al. prepared 2D SnS nanosheets using liquid metal solutions for the advanced and controlled synthesis.[157] Low melting point metals such as Bi and In were used to dope 2D SnS to tune optoelectronics properties, resulting in 22.6% increase in piezoelectric coefficient for optimized structure. More recently, Peng et al. synthesized new 2D binary M_8X_{12} monolayer where M is Mo or W and X is S, Se, or Te via CVD methods.[158] They found that Mo_8S_{12}, Mo_8Se_{12}, W_8S_{12}, and W_8Se_{12} monolayers exhibit direct band gaps and great optical absorption properties in the visible region, while Mo_8Te_{12} and W_8Te_{12} monolayers show metallic function. In particular, 2D monolayer W_8Se_{12} induces a direct−indirect-metal transition under uniaxial strain. Bahti et al. investigated electronic and optical properties of 2D AlMSTe monolayers where M is Ga or In via Density Functional Theory and First-principle molecular dynamic simulations.[159] They revealed that the AlGaSTe and AlInSTe monolayers exhibited direct and indirect bandgap of about 2.23 and 2.69 eV, respectively, and they showed strong visible-region absorption properties. These monolayers offer great possibility for promising optoelectronics and photocatalytic applications due their great thermodynamic stability.

2.2. 1D Nanomaterials

2.2.1. NWs

Recently, the 1D NWs have attracted much attention for next-generation in the area of optoelectronics because of promising applications due to their unique confinement effect which is dependent on materials size (photons and electrons) and distinct advantage of structural features such as large aspect ratio.[160–162] Depending on the electronic features and the ratio of chemical composition, 1D NWs based layer can be used to metallic conductor layer, dielectric layer, and semiconductor layer. In particular, semiconductor NWs are promising materials for optoelectronic sensor and PDs because of their optical transitions related to the intrinsic bandgap difference.[61,163,164] Because of good optoelectronic properties of IV, II–VI, and III–V semiconductor materials composition and facile fabrication process, various combinations such as GeS, GaS,[165] CdS, CdSe, ZnO,[166] and Sb-based materials have been studied.[164,167–169] At first, II–VI based semiconductor NWs are generally used for diverse applications because they have many advantages such as good electron mobility, cheap price, various fabrication methods, and low temperature processability.[163,170,171] Among them, ZnO is generally used for photonic sensors and UV PDs. And III–V based semiconductor materials exhibit simple and wide tunable bandgap, high electron mobility, and low leakage current. Also, they show good EQE and high responsivity owing to large surface-to-volume ratio generally induced from plenty of trap states in the oxygen vacancies. Especially, Sb-based III–V semiconductor NWs such as GaAsSb show good bandgap tunability via simple controllable composition ratio.[60,172,173] GaAsSb widely covers in the near-infrared (NIR) region because bandgap can be easily tuned from 0.726 to 1.43eV at room temperature.

Moreover, different synthesis methods of 1D NWs were explored to improve tunable parameters and architecture stability. In general, homogeneous structured NWs show good optical and electrical properties such as good photon confinement effect, easy synthesis process, and low power consumption.[172,174,177,178] Moreover, diverse heterostructure NWs such as branch-like,

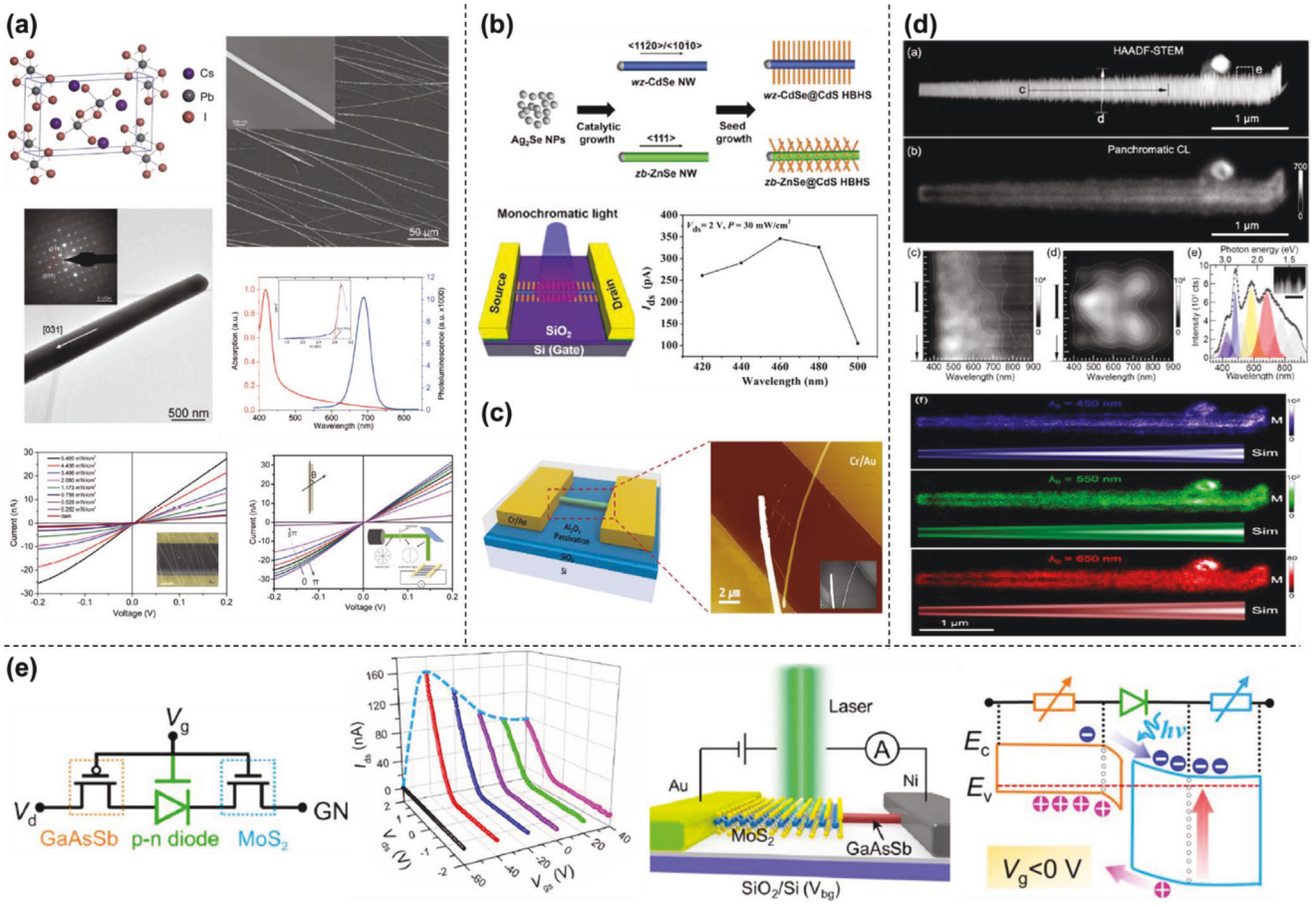

Figure 5. a) Diagrammatic crystal structure of $CsPbI_3$, exhibiting obviously different lattice parameters at three directions. The SEM and TEM images of nano wire correspond optical characteristics. Reproduced with permission.[162] Copyright 2018, Wiley-VCH. b) Synthesis of two types of hyperbranched heterostructures with different architectures. And the schematic of phototransistor device with the dependences of the photocurrent on the incident wavelength of a single wz-CdSe@CdS HBHS phototransistor. Reproduced with permission.[174] Copyright 2021, Wiley-VCH. c) Schematic illustration of the $Ta_2Ni_3Se_8$ nanowire field effect transistors and the atomic force microscopy image of the device. Reproduced with permission.[175] Copyright 2021, Wiley-VCH. d) STEM-cathodoluminescence spectroscopy on individual type GaS nanowires ($T = 103$ K). Monochromatic cathodoluminescence maps (bandwidth 50 nm) of the GaS nanowire for (free-space) center wavelengths $\lambda_0 = 450$, 550, and 650 nm. "M": measured intensity maps. "Sim": simulated intensity distribution. Reproduced with permission.[165] Copyright 2020, American Chemical Society. e) The mixed-dimensional anti-ambipolar phototransistors based on 1D GaAsSb/2D MoS_2 heterojunctions. Reproduced with permission.[176] Copyright 2020, American Chemical Society.

core/shell, hybrid and multiblock structures have been developed for enhancing optoelectronic parameters. Zhou et al. described a PD based on cesium lead iodide (β-$CsPbI_3$) NW array with anisotropic crystal structure that exhibits high sensitivity to linearly polarized light with a photocurrent anisotropy ratio of 2.68 and 2.17 on rigid and flexible substrates, respectively, and excellent flexibility and folding endurance of the device (**Figure 5**a).[162] The anisotropic $CsPbI_3$ NWs used in the PD may have applications in novel optoelectronic devices.

Li et al. prepared seeded grown CdS NWs with hyperbranched heterostructures (HBHSs) on abundant interfaces.[174] The two types of HBHSs were successfully synthesized by catalytic growth and seed growth method on the wz-CdSe NW and zb-ZnSe NW, respectively as shown in Figure 5b. As result, wz-CdSe@CdS and zb-ZnSe@CdS HBHSs NWs were examined as optoelectronic devices. The 1D wz-CdSe@CdS HBHS phototransistor exhibited a maximum photocurrent value about 350 pA, time-resolved photoresponse of 67.8 mW cm^{-2}, and good photocurrent switching ($I_{on}/I_{off} > 50$) in the wavelength of 460 nm. Also, the optoelectronic performance of phototransistor based on zb-ZnSe@CdS showed similar behaviors with above results. Choi et al. investigated a method for synthesizing 1D HBHSs with desired spatial architecture and specific interfaces using a seeded growth approach.[175] These HBHSs consist of CdS branches growing on 1D NW trunks with different growth behaviors, and their composition can be tuned using cation exchange. The resulting optoelectronic devices based on a single HBHS exhibited better photoresponse performance than a single NW trunk, and this work offers a platform for exploring the potential applications of HBHSs for photo harvesting and conversion (Figure 5c). Wang et al. developed $CsPbX_3$ (X = Cl, Br, I) based perovskite NWs which can be synthesized at room temperature with the diameter of 2–3 nm and length up to several hundreds of nanometers.[162] In particular, $CsPbBr_3$ NWs were maintained in the transformation process into NRs with tunable shorter lengths and thicker diameters. The polarization-sensitive

photodetection performance of $CsPbBr_3$ NW film was 0.6 mW cm^{-2} in the wavelength of 453 nm. This approach enables 1D NW-based PDs to tune optoelectronic characteristics efficiently and offer simple and cheap method for utilizing PD applications. In order to improve the optoelectronic properties, diverse growth methods for synthesis of 1D NWs were demonstrated. Sutter et al. examined 1D NWs from 2D layered crystals by integrating vdW epitaxy with vapor-liquid-solid (VLS) growth.[165] They attained vdW based GeS NWs with diameter about 15 nm maintaining tens of μm length via VLS growth over Bi catalysts. As a result, individual NWs showed a blue shift of the band-edge luminescence to photon energy of 2.4 eV (bulk GeS : 1.6 eV) in accordance with a bandgap opening owing to quantum confinement in the thin-film vdWs NWs (Figure 5d). Further, Wang et al. prepared an anti-ambipolar PDs using the vdW bonding of a 1D p-type GaAsSb NW and a 2D n-type MoS_2 nanoflake (Figure 5e).[176] The device showed anti-ambipolar behavior when operated as a three-terminal field-effect transistor and electrical and optoelectronic properties were studied through gate modulation. The PD was also demonstrated to have good imaging capabilities as a single-pixel in a high-resolution visible image sensor. These features show the versatility of mixed-dimensional vdW heterostructures in next-generation electronics and optoelectronics.

2.2.2. NRs

1D semiconductor NRs have various unique qualities, such as polarized light emission, low lasing threshold, and great charge transport, which can set them apart from other nanostructured semiconductor. The 1D feature of semiconductor NRs promotes effective charge separation and enables precise material deposition, leading to the creation of 1D heterostructures with exceptional potential in fields such as optoelectronics and photocatalysis.[179–182] Until now, various methods for synthesizing NRs have been developed, despite the lack of maturity in the most established method. Techniques such as carbon nanotube-assisted template-mediated growth, solution-liquid-solid growth, solvothermal process, and solution-based colloidal NRs growth have been investigated to produce NRs with different sizes, shapes, and qualities.[183–186] In particular, methods for producing metal halide perovskite NRs include high-temperature (hot-injection and solvothermal), low-temperature (ligand-assisted reprecipitation and spin-coating), reshaping (top-down and bottom-up), solid-state synthesis, and template-mediated synthesis. The hot-injection method is a popular way to synthesize colloidal NRs, including CdS and CdTe based devices and others, allowing size and shape adjustments for optimized properties in various applications. The hot-injection method can produce high-quality perovskite NRs, but it is challenging to quickly attain the desired shapes and properties. The solvothermal method, however, is faster (seconds to minutes), has a lower rate of crystal growth, and enables better control of the desired properties. The ligand-assisted reprecipitation process (LARP) uses ligands to promote the formation of perovskite NRs.[187] Unlike the hot-injection method, LARP is simple to implement, enables in low temperatures, and allows for easy control of the properties by adjusting the ligand parameters. Spin-coating and post-treatment methods allow for the synthesis of perovskite thin films with NR morphologies. This is achieved by depositing two precursor solutions of different polarities on the substrate. The first solution is BX_2 in a polar solvent, followed by the second solution of AX in an antisolvent. This two-step deposition process results in the crystallization of ABX_3 perovskite films with NR morphology. In addition, both top-down and bottom-up approaches aim to reshape perovskite nanostructures, but top-down approaches are more commonly used due to their ease of accessibility through straightforward colloidal synthesis. The solid-state synthesis of metal halide perovskite NRs can reduce the use of toxic solvents compared to wet chemistry synthesis, making it a more environmentally friendly option for industrialization.[188] This method involves a chemical reaction between solid materials, which is facilitated by the application of mechanical force. Template-mediated synthesis is a simple and efficient method for producing perovskite NRs by impregnating perovskite precursor solution into rod-shaped templates such as silicon NRs and NT structures. The size of the perovskite NRs can be controlled by the size of the template without affecting the crystal structure.[181]

Various NR growth methods and synthetic types of materials are being developed to be used in PDs. Cao et al. used a new self-powered PD based on a core–shell InN/In_2S_3 NR array with an ultrafast response speed, which exhibits an excellent photovoltaic responsivity, detectivity, high current on/off ratio, and fast rise/fall time of 22/32 μs.[33] The device was synthesized on Si substrates as shown in **Figure 6**a via a two-step method and has great potential for electronic applications. Zhang et al. prepared a strategy for maintaining ultrastable color purity in organic optoelectronic devices through the use of self-assembled organic micro/nanocrystals.[186] The study demonstrated the effect of crystallization on suppressing the formation of long-wavelength green band defects in fluorene-based blue emitter, resulting in stable deep-blue emission (Figure 6b). Lin et al. investigated new methods for efficient piezo-photocatalytic hydrogen evolution from water splitting, which have been developed using 1D NR-structured $Cd_xZn_{1-x}S$ (x = 0, 0.2, 0.4, 0.6, 0.8, and 1) solid solutions, which demonstrate a synergistic effect of simultaneously converting solar and vibration energy, resulting in a prominently enhanced H_2 yield rate of 4.45 mmol g^{-1} h^{-1}.[188] The increased catalytic activity of $Cd_{0.4}Zn_{0.6}S$ is attributed to strengthened charge separation by piezo-potential, increased strain sensitivity, and desirable optimization between piezoelectricity and visible-light response due to the formation of 1D configuration and solid solution (Figure 6c). Cao et al. reported Sb_2Se_3 NR arrays using a close-spaced sublimation method with a highly preferred (002) orientation (Figure 6d).[189] The NR arrays showed a higher photocurrent due to improved carrier transport efficiency and light-trapping ability compared to Sb_2Se_3 thin films. In addition, boron-doped ZnO/Sb_2Se_3 NR array heterostructure PDs showed excellent performance in the 460–930 nm wavelength range, with the best performance seen under 625 nm light. The defect density of the Sb_2Se_3 layer was also suppressed to improve device performance, as seen through numerical simulation of the device. You et al. synthesized PbSe NRs with an unconventional anisotropy by using bcc-Ag_2Se as a catalyst through the solution-solid-solid growth model at 250 °C for 20 s.[185] They investigated the reaction and growth mechanism of the NRs under different experimental conditions. The high quality of the NRs was used

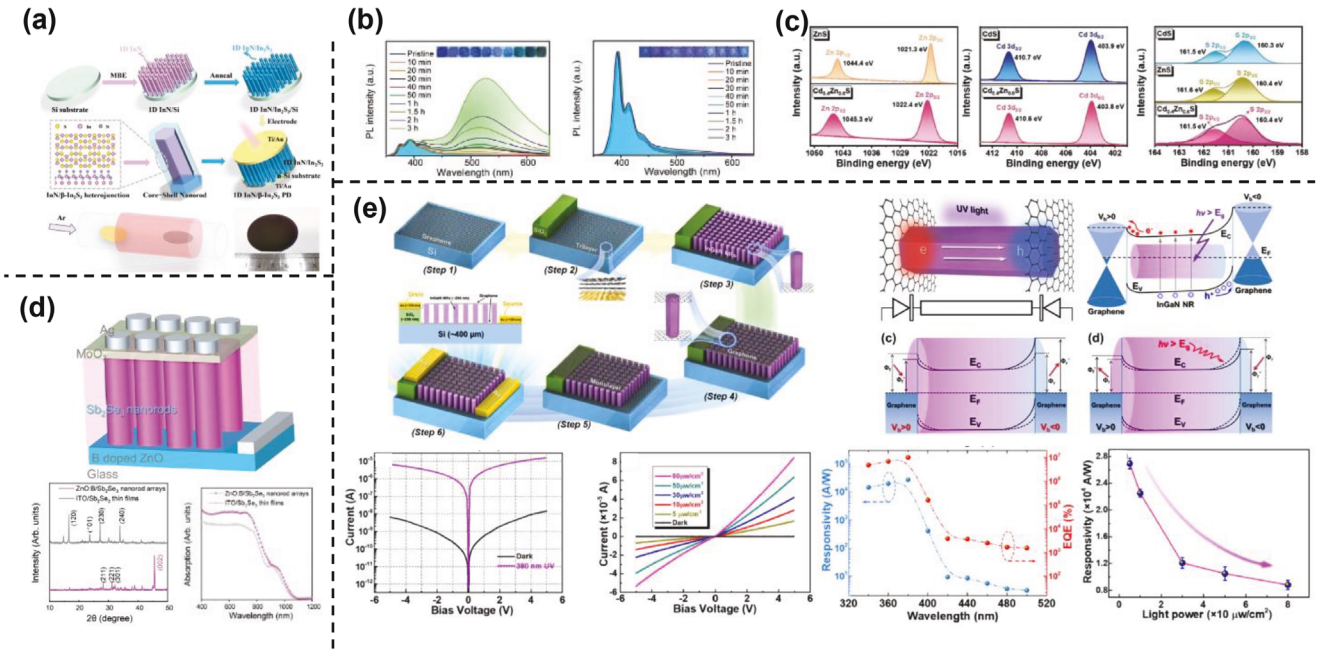

Figure 6. a) Schematic diagram of the procedures for the synthesis of InN and InN/In_2S_3 core–shell nanorod array photodetectors. Reproduced with permission.[33] Copyright 2022, Wiley-VCH. b) The photoluminescence spectra about UV-irradiation stability of amorphous film and crystalline nanorod film with different UV-irradiation times; inset: the photographs of films. Reproduced with permission.[186] Copyright 2022, Wiley-VCH. c) High-resolution XPS spectra of Zn 2p, Cd 3d, and S 2p of ZnS, $Cd_{0.4}Zn_{0.6}S$, and CdS based 1D NRs. Reproduced with permission.[188] Copyright 2021, Wiley-VCH. d) Device schematic and performances (absorption spectra and XRD data) of the ZnO:B/Sb_2Se_3 heterostructure based photodetectors. Reproduced with permission.[189] Copyright 2022, Wiley-VCH. e) Schematic for the fabrication process and working principle of an integrated hybrid graphene/InGaN NRAs/graphene UV PDs. And corresponding optoelectronic characteristics. Reproduced with permission.[182] Copyright 2019, American Chemical Society.

to make a simple solution-processed PD with a broadband detection ability from 405 to 1064 nm, showing high responsivity of 0.78 A W^{-1} and fast response time of 17.5 μs. This work confirms the solution-solid-solid mechanism for the preparation of group IV–VI semiconductor-based NRs and provides an alternative way to make high-performance PDs. Zheng et al. demonstrated a self-integrated hybrid UV PD based on InGaN NR arrays sandwiched between transparent graphene contacts forming a Schottky junction has been demonstrated.[182] The hybrid system exhibits ultrafast response time and superhigh photosensitivity, and it is believed to have great potential for next-generation integrated 1D/2D nano-based optoelectronic and photodetection devices (Figure 6e).

2.2.3. NTs

TMDC vdW 1D heterostructured NTs are synthesized from 2D nanosheets, providing new opportunities for potential applications in electronics and optoelectronics. 1D heterostructured TMDCs, combined with single-walled carbon nanotubes (SWCNT)[190,63] and boron nitride[191] NTs etc.,[192–194] demonstrate improved functionality compared to 2D TMDC nanosheets in electronic and optoelectronic devices.[195,178] Recent researches show that 2D structures can self-assemble into NT structures, expanding the possibilities for their applications.[196–198] Among them, the unique structure of carbon NTs facilitates excellent mechanical, physical, and chemical properties, leading to high interest and expectations for potential applications.[199,200] TMDC NTs have unique electrical and optical properties, including a small band gap and diameter-dependent band gap behavior, making them useful in photovoltaic devices.[64,36] The bandgap can be direct for zigzag-type TMDC-SWCNTs and indirect for armchair type TMDC-SWCNTs. In addition, high-purity single-chirality SWCNTs show great potential in photoelectric devices due to their high photoelectric properties. Advancements in separation techniques make it possible to separate large amounts of single-chirality SWCNTs, laying a foundation for future optoelectronic devices such as PDs, biological imaging, and light emission devices. Furthermore, the efficient photoresponse of single-chirality SWCNTs is due to their unique optoelectronic structure, which leads to wavelength-dependent photoresponse. This makes them a promising candidate for high-performance PDs in various applications. Also, double-wall (DW) MoS_2-NTs have been largely researched because band alignment and energy band gap can be easily adjusted by varying diameter, resulting in changes in open-circuit voltage, short-circuit current, and power conversion efficiency. The photoelectric properties of DW MoS_2-NTs are optimal, making them a promising material for high-performance TMDC NT-based optoelectronic devices.

Chithaiah et al. developed a reproducible synthetic route for the production of highly crystalline pure-phase MoS_2 NTs via a multistep vapor-gas-solid (VGS) process, without the assistance of a catalyst and in a scalable fashion (**Figure 7**a).[201] The growth

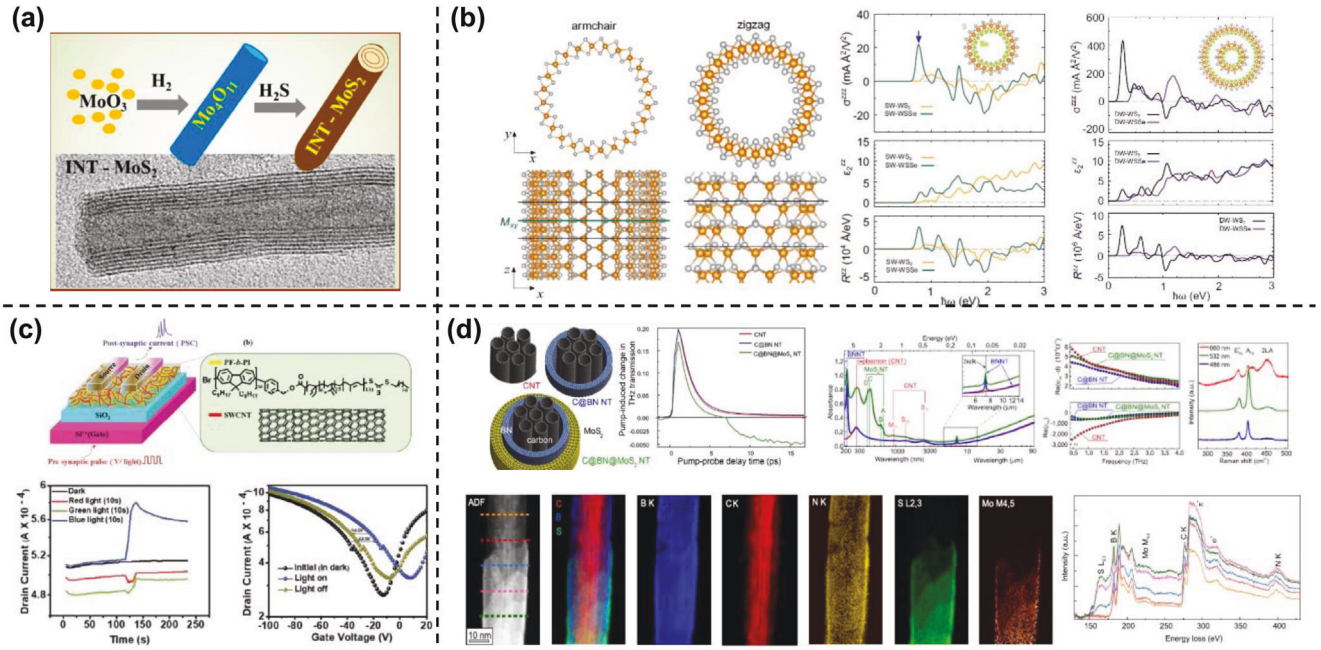

Figure 7. a) Schematic diagram of MoS_2 nanotubes synthetic enigma: the futile attempts to synthesize inorganic nanotubes of MoS_2 via vapor–gas–solid reaction. Reproduced with permission.[201] Copyright 2020, American Chemical Society. b) Atomic structure and electric polarization of TMDC SWCNTs and the photovoltaic effect of Janus-type WSSe nanotubes in comparison with that of WS_2 nanotubes. Reproduced with permission.[193] Copyright 2022, Nature Publishing Group. c) Schematic of designed bottom-gate top-contact organic field-effect transistors, synaptic thin-film transistors, and chemical structure of PF-*b*-PI and schematic of SWCNT structure with charge retention in dark (black) and when red (λ = 640–660 nm), green (λ = 522–542 nm), and blue (λ = 395–415 nm) lights were pulsed for 10 s, as indicated in red, green, and blue, respectively (V_{DS} = -60). Reproduced with permission.[200] Copyright 2022, Wiley-VCH. d) Device schematic and performances of 1D vdW heterostructures comprising carbon nanotubes wrapped by atomically thin nanotubes of boron nitride and MoS_2. Reproduced with permission.[195] Copyright 2020, American Chemical Society.

mechanism involves separating the reaction into five steps and using a horizontal reactor with a porous-quartz reaction cell to create proper quasi-static conditions for the reaction. The resulting inorganic nanotubes (INT)-MoS_2 offers a platform for potential applications in the field of optoelectronics and reinforcement of polymer composites. Tang et al. also developed MoSSe NTs based on density functional calculations which showed that Janus armchair MoSSe NTs are energetically favored and easier to synthesize compared to zigzag NTs.[196] The electronic structures and optical properties of Janus armchair MoSSe NTs depend on the radius, with small radius NTs being indirect semiconductors and larger radius NTs having direct band gaps in the range from 1.49 to 1.62 eV. Kim et al. proposed 1D TMDC NTs which produce a spontaneous photocurrent, which is not possible in their higher-dimensional counterparts.[193] WS_2 NTs exhibited a giant shift current near the infrared region, and a Janus-type heteroatomic configuration can maximize this interwall effect, providing a basis for a complete quantum mechanical understanding of the light-matter interaction in the geometric characteristics of reduced dimensions (Figure 7b). Mburu et al. prepared simple-structured synaptic PDs using toluene-based solution of poly(9,9-dioctylfluorene)-b-polyisoprene (PF-b-PI)-wrapped SWCNTs.[200] The device exhibited high charge carrier mobility and output current and it can be independently modulated by either photonic or electric signals. The SWCNTs act as a semiconducting layer while PF-b-PI enables charge trapping to achieve a large memory window suitable for memory devices. In particular, dual photonic and electrical device operation may pave the way for the design of carbon-based semiconductor materials for neuromorphic vision systems (Figure 7c). Also, Xu et al. reported synthesis of Te NTs with different diameters and hexagonal phase along the [001] direction with a solvothermal method.[197] A single NT with a diameter of 40 nm was used to fabricate Te PDs using a focused ion beam (FIB) technique. The PDs exhibited a high responsivity of 1.65×10^4 A W^{-1} and a photoconductivity gain of 5.0×10^6%. This study provides a promising and effective method for the preparation of PDs based on 1D nanostructures, which has the potential to improve the application of 1D semiconductive nanostructures in the production of high-performance optoelectronic devices. Burdanova et al. reported the structure, composition, and optoelectronic properties of 1D vdW heterostructures comprising carbon NTs wrapped by atomically thin NTs of boron nitride and molybdenum disulfide as displayed in Figure 7d.[195] Ultrafast pump-probe spectroscopy identified that, in the MoS_2 NTs, excitons coexisted with a prominent population of free charges, and the electron mobility was comparable to that found in high-quality atomically thin crystals, highlighting the potential of 1D vdW heterostructures for nanoscale optoelectronic devices.

2.3. 0D Nanomaterials

0D NPs can improve the performance of optoelectronic devices in several ways, such as enhancing the electrical conductivity,

suppressing the recombination of charge carriers, and reducing the charge carrier recombination loss.[65,202] In particular, carbon NPs (CNPs) have been shown to improve the efficiency and stability of PDs, and also offer potential for customization of optoelectronic properties, making them a promising option for future developments in this field. CNPs, such as graphene quantum dots (GQDs),[66,67,203–206] carbon dots (CDs),[207] and polymer dots,[208] have garnered attention due to their cheap, environmentally friendly synthesis methods, easy functionalization, tunable visible-to-NIR emission with high photoluminescence quantum yields, ability to be processed into large area thin films, and nontoxic nature, making them promising for opto- and bioapplications. The synthesis of CNPs can be achieved through top-down or bottom-up methods.[65] GQDs are the most highly carbonized type of CNPs and usually contain 1–3 layers of graphene with a size smaller than 10 nm. Their bandgap or transition energy can be adjusted from 0 eV (graphene) to approximately 6 eV (benzene) by varying their size, doping, and surface/edge functional groups such as oxygen or nitrogen.[209] The electron confinement energy in GQDs can be expressed using the Dirac Fermion model,[210] such as

$$\Delta E_c = E_{g(el)}^{GQD} - E_{g(el)}^{Bulk} = \pi \hbar v_f / L \approx 2/L$$

where v_f is the Fermi velocity of electrons in graphene and L is the lateral size of GQDs. The energy bandgap for bulk graphene $E_{g(el)}^{Bulk}$ is zero, and the $E_{g(el)}^{GQD}$ can be expressed as inversely proportional to GQD lateral size. This model predicts that the energy bandgap for GQDs should be inversely proportional to their lateral size. The shape of sp^2-domains may also affect the energy levels.

The CDs are usually considered as sp^2-areas of polyaromatic hydrocarbons located within a sp^3-hybridized carbon matrix.[211] They typically display similar trends in HOMO–LUMO energy levels as GQDs, including being impacted by the size of the sp2-areas and the surface modification. Just like GQDs, the HOMO–LUMO gap decreases as the size of the CDs increases. The electronic makeup of the CDs can also be greatly influenced by doping and surface modification.[203] Additionally, polymer dots are usually created from organic components through a low-temperature reaction process, resulting in having the lowest carbonization degree among the CNP family.[65] Comprised of short polymer chains and abundant functional groups, polymer dots have a highly crosslinked network structure. Polymer dots can also be generated by crosslinking GQDs with polymer chains, in which case they would exhibit similar energy structures and optical responses as GQDs. **Figure 8** illustrates the remarkable performance of 0D materials in PDs, highlighting their exceptional responsivity and detectivity.

The use of 0D NPs has been shown to improve the performance of PDs by influencing the extraction and transport of charge carriers, promoting crystallization, allowing for efficient passivation, blocking ion migration, suppressing hysteresis, and enhancing environmental stability.[213,214] Arafat et al. synthesized $Co_{9-x}Ni_xS_8$ NPs with different Ni content ($x = 2.6$, 3, and 3.4) using a solvothermal method.[202] Figure 8a shows the corresponding results. Spectroscopic analysis showed that Ni ions were integrated into the Co_9S_8 lattice in some samples, while others showed segregation of Co ions forming an oxide phase. The bandgap of $Co_{9-x}Ni_xS_8$ decreased with higher Ni content, and the sample with the lowest Ni content ($x = 2.6$) had the highest refractive index. The highest photoluminescence emission was observed in the sample with $x = 3.0$ due to the presence of a secondary phase (Co_3O_4) that increased the number of defect levels for trapping more excited electrons. Chen et al. proposed a method of using multidentate ethylenediaminetetraacetic acid (EDTA) to resurface perovskite QDs and improve their performance in optical electronics (Figure 8b).[212] The EDTA chelates the suspended Pb^{2+} ions on the perovskite QD surfaces and passivates the surface defects to suppress nonradiative recombination. It also crosslinks QDs to improve their electronic coupling and facilitate charge carrier transport. This resulted in a power conversion efficiency of up to 15.25%, one of the highest for inorganic $CsPbI_3$ QD optoelectronics. The method also showed good stability. The improved performance of the PDs was due to improved charge carrier extraction and enhanced electronic coupling of the QDs.[212,215,216]

Research is being conducted to improve the optical properties of PDs by changing the constituent materials and structures using heterojunction structures. Tang et al. present the fabrication of dual-band PDs using two stacked photodiodes made of different-sized HgTe QDs.[217] The HgTe QDs were designed in a n–p–n configuration and doped with Ag_2Te and Bi_2Se_3 to produce p- and n-doping at the interfaces. The two different sizes of HgTe QDs were chosen to cover short-wave infrared (<2.5 μm) and mid-wave infrared (3–5 μm) spectra. The dual-band detector was shown to be rapidly switchable between short-wave and mid-wave infrared modes and was used to produce imaging applications. The response of the two bands can be calibrated to determine the absolute temperature of objects. This study highlights the potential for HgTe QDs to be used in infrared technology applications. Dong et al. presented a simple method to control the morphology of a poly(3-hexylthiophene):HgTe QD hybrid phototransistor for efficient infrared photodetection.[218] The combination of the two materials showed improved charge transport, response speed, noise level, and sensitivity compared to conventional phototransistors. The results showed high detectivity and fast response time under room temperature, making it a promising solution for the commercialization of low-cost infrared PDs that can be integrated with silicon technology. Chen et al. explored a new method to passivate large-sized PbS QDs by using halide perovskite.[219] By adding a small amount of CsI to the classic PbX_2 ligand solution, the perovskite-passivated QD film was obtained with reduced defect states and improved stability compared to the control halide-passivated QD film. The perovskite-passivated QD PDs showed improved EQE, lower dark current density, and better stability compared to the pristine QD based PDs, providing the best balance of detectivity and speed among reported QD-based PDs. This study provides a promising alternative for preparing high-quality QDs for various applications, such as light-emitting diodes, tandem cells, and PDs.[220,122,221] Furthermore, Kim et al. recently presented high-resolution active-matrix driving of color-selective PD arrays based on vertically stacked three different-sized/color (red, green, and blue) QDs with low-temperature solution-processed amorphous oxide semiconductor indium-gallium-zinc-oxide (IGZO) (Figure 8c).[72] The vertically stacked full-color QD PDs with very high density of 5500 devices cm^{-2} were successfully implemented on ultrathin

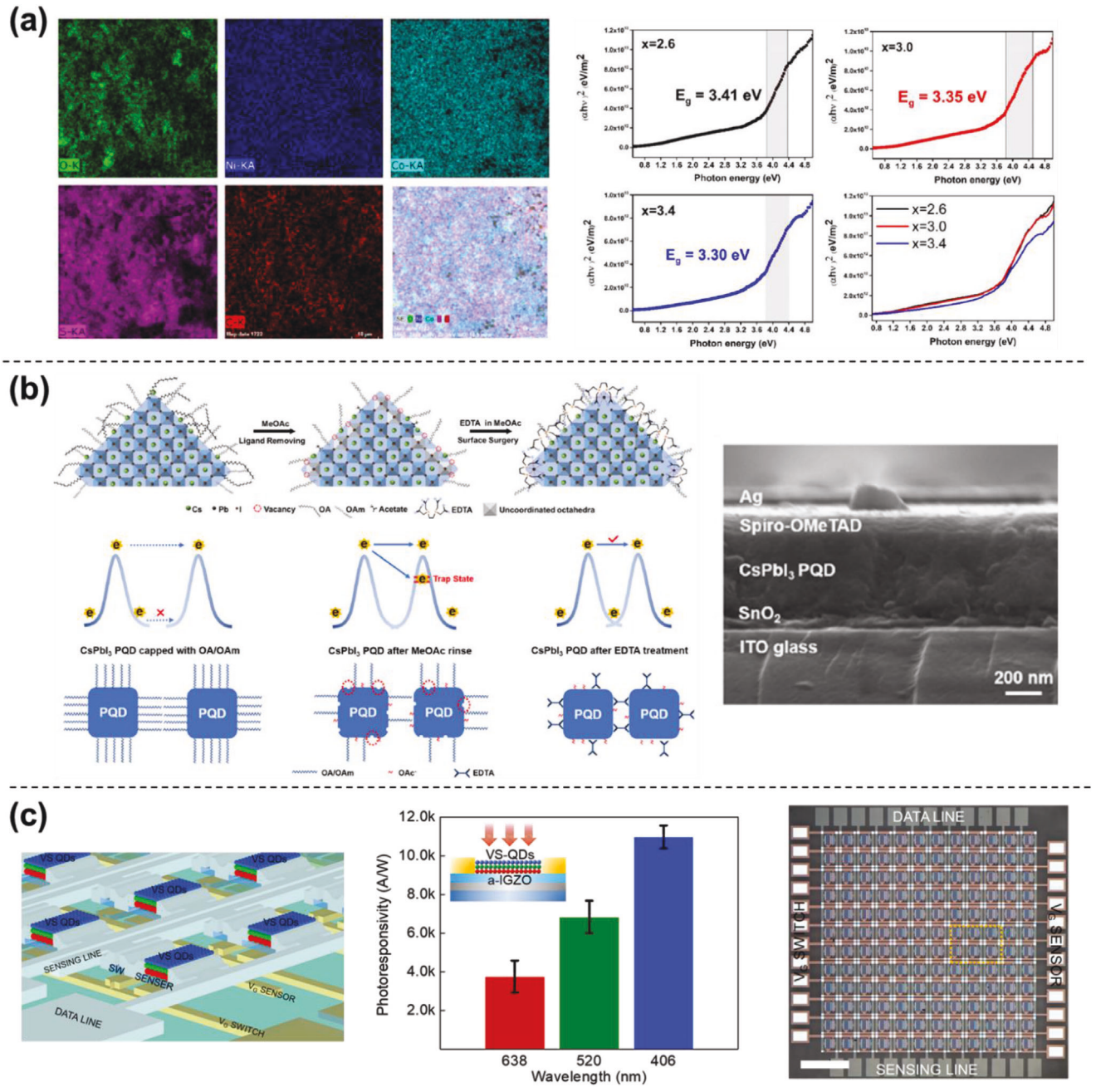

Figure 8. a) The $Co_{6.4}Ni_{2.6}S_8$ nanoparticles for optoelectronic applications corresponding elemental mapping with all constituents (O, Ni, Co, Co, S, and C). And the plots for bandgap energy of $Co_{9-x}Ni_xS_8$ with different Ni amounts (x = 2.6, 3, and 3.4). Reproduced with permission.[202] Copyright 2020, Elsevier. b) Schematic diagram of surface surgery treatment of perovskite QDs using EDTA molecules. The electrical coupling between the adjacent perovskite QDs in the oleic acid/oleyl-amine, methyl acetate and EDTA based perovskite QD solid films. Reproduced with permission.[212] Copyright 2022, Elsevier. c) Vertically stacked QD/IGZO phototransistor array. Relevant light intensity profile was reconstructed from output current mapping of 12 × 12 photodetector array. Reproduced with permission.[72] Copyright 2021, Wiley-VCH.

flexible polymeric substrates, which exhibit ultrahigh photoresponsivity of more than 1×10^4 A W^{-1} and photodetectivity of 1.1×10^{18} Jones as well as wide dynamic ranges (>150 dB). The proven results show that low-dimensional nanomaterial such as QD-based PDs can offer promising impact on multispectral and conformal multiplexed compatibility for state-of-the-art photonic and optoelectronic image sensing applications.

3. Photodetector Applications

3.1. Photodiodes, Photoconductor, and Phototransistors

To date, various types of PDs, including photodiodes, photoconductors, and phototransistors, have been developed. Each of these devices utilizes different operating principles and has

its own advantages and disadvantages. Among them, p–n junction photodiodes consist of semiconductors with opposite conductivity types.[217,222–224] The photovoltaic effect drives the photoresponse in p–n junction PDs.[108] Normally, p–n photodiodes exhibit rectifying behavior, meaning they have an asymmetric current-voltage characteristic in the dark. When exposed to light, the semiconductors absorb photons with energy above their bandgap, producing electron-hole pairs. These electron–hole pairs form within a diffusion length from the junction, then migrate to the space charge region where they are separated by a built-in electric field and transported in opposite directions, leading to a large photocurrent.[173,225]

P–n/Schottky photodiodes have two modes of operation.[221,226–228] The first mode is the photovoltaic mode, which operates with zero bias, and typically has a relatively low dark current, resulting in improved specific detectivity. The second mode is the photoconductive mode, which operates under reverse bias and has a faster response speed compared to photoconductors due to lower diode capacitance and reduced transit time. However, photodiodes have lower EQE and responsivity. For visible imaging, silicon photodiodes are typically used as they can be monolithically integrated with silicon readout integrated circuits (ROICs), leading to low-cost and high-performance imagers. On the other hand, infrared imagers commonly use PDs made of InGaAs, InSb, or HgCdTe,[229] but they require high-quality single-crystalline substrates and high-temperature vacuum processing, preventing direct integration with silicon ROICs. To address this issue, NIR imagers that integrate low-dimensional nanomaterial-based photodiodes and a large-scale ROIC using CMOS structures have been developed. The design and fabrication of photodiodes are optimized for CMOS compatibility, high homogeneity, low dark current density, and high EQE.[167,227,230]

Photoconductors consist of a light-absorbing layer and ohmic contact electrodes, making their fabrication process simpler compared to photodiodes and phototransistors.[80,231–234] These devices require an external power source to drive photoexcited electrons and holes in opposite directions, leading to a high photoconductive gain, large EQE, and high responsivity.[218,235,236] However, the high dark current and slow response speed of photoconductors limit their use in certain fields such as light communication and photoswitching. To overcome these limitations and improve performance, the following researches are being actively conducted. 1) Hybrid photoconductors: there has been a growing interest in the development of hybrid photoconductors that combine the benefits of different materials to achieve improved performance. Examples of hybrid photoconductors include the integration of graphene with traditional photoconductive materials such as GaAs and Si. 2) Non-toxic photoconductors: research in this area is focused on finding alternative materials with similar properties to traditional photoconductive materials, but without the toxic components. 3) Flexible photoconductors: the development of flexible photoconductors is becoming increasingly important in the field of wearable and flexible electronics. Research in this area is focused on finding materials and processing methods that allow for the creation of flexible photoconductive devices with high performance and stability. 4) Low-dimensional nanomaterial-based photoconductors: the use of low-dimensional nanomaterials in photoconductors is an emerging trend. Research in this area is focused on developing photoconductors with improved performance and stability through the use of low-dimensional nanomaterials.

Phototransistors consist of semiconducting channel materials, dielectrics, and conductors such as source, drain, and gate electrodes.[111,237] The charge transport can be controlled by a gate voltage and modulated by light, leading to a large photocurrent and photoresponsivity.[176,238,206] With a high EQE of over 100%, phototransistors have broad application potential in fields such as light communication and PDs. Recent trends in phototransistors focus on developing high-performance devices with improved response speed and efficiency. This is achieved through the use of novel nanomaterials and heterostructures, such as 2D materials, perovskites, and hybrid nanostructures.[112,230,233,239,240]

The important figure of merits for PDs has been summarized in **Table 1** below. Table 1 represents the performance comparison of PDs of different low-dimensional nanomaterials which have been reviewed in this paper.

3.2. Neuromorphic Devices

Neuromorphic devices offer a new approach to electronic artificial intelligence (AI) by allowing for the implementation of synaptic functions at the hardware level.[250–254] This helps to overcome the limitations imposed by traditional computing systems. Further, optoelectronic neuromorphic devices exhibit a new approach to synapse implementation in artificial electronic devices.[255,256] By combining photosensitivity and synaptic plasticity in a single device, these devices can achieve higher computing speeds, wider bandwidths, reduced crosstalk, and more efficient energy consumption compared to traditional electronic synaptic devices. Among various materials with unique functionalities for optoelectronic neuromorphics, low-dimensional nanomaterials stand out for their exceptional optical and electrical properties. These materials can easily be utilized in the construction of vdW heterostructures, which have desirable surface characteristics.

Optoelectronic synaptic devices provide the potential to create a new type of AI that can process and store visual signals in a highly efficient manner such as optical neuromorphic logic computing, visual sensors, and learning algorithm.[206,255,257] They also allow for the stimulation of neural activities and synaptic functions from multiple dimensions, advancing the development of more intelligent neuromorphic devices. The human brain performs such computations in a parallel or hierarchical manner with efficient power consumption, and optoelectronic synapses have the potential to emulate this behavior by incorporating logic functions.[256,258] With their high bandwidth, fast speed, robustness, and low crosstalk, optical inputs in optoelectronic synapses overcome the limitations of electrical inputs, significantly enhancing the information processing capability for neuromorphic computing. Recent advancements have led to the successful implementation of several typical logic functions such as AND, NAND, OR, and NOR in optoelectronic synaptic devices. Also, optical information can be converted into neural actions by neuromorphic devices, enabling the creation of a vision system in the visual cortex. This results in a more energy-efficient and high-speed processing of visual information compared to traditional

Table 1. Performance comparison of photodetectors (PDs) of different low-dimensional nanomaterials.

Dimension	Materials	λ [μm]	Responsivity [A W^{-1}]	EQE [%]	Response time [ms]	Detectivity [Jones]	Refs.
2D	Graphene	0.78–1.5	9197	11.5	0.275	–	[91]
	Graphene	1.5	0.1	64	< 0.1	–	[92]
	Graphene	10.6	≈5	ss	<4.2	3.6×10^5	[88]
	Graphene	1.55	240	–	–	3.4×10^{12}	[83]
	Graphene	0.47-27.12	5.36	–	68	1.57×10^9	[87]
	Graphene/tellurium	<2	1.04×10^9	6	0.028	3.69×10^8	[89]
	Graphene/PTCDA/pentacene	0.5~0.67	$\approx 10^4$	9	< 0.028	–	[90]
	NPMLgraphene-$FeCl_3$	1.3–12	6.15×10^3 (V/W)		0.0001	2.3×10^9	[90]
	MoS_2	0.45–0.97	29	7.8	300	$\approx 10^9$	[102]
	$MoSe_2$-WSe_2	0.52	110	23.4	–	10^9	[108]
	$Cs_3Cu_2I_5$	0.27	3.78	≈2	163	–	[125]
	$Cs_2Pb(SCN)_2Br_2/MoS_2$	0.3–0.8	1.22×10^5	8.99	165	1.16×10^{14}	[123]
	BP/Bi_2O_2Se	1.3	0.89	84	0.118	1.14×10^{10}	[145]
	BP/MoS_2	0.365	77.16	200	–	6.5×10^9	[144]
	$CsPbCl_3$	0.44, 0.98	1.96, 0.12	–	–	5×10^{12},2.15×10^9	[124]
	$(CH_3(CH_2)_3NH_3)_2(CH_3NH_3)_3Pb_4I_{13}$	0.63	0.53	103	17	3.24×10^{13}	[130]
	$CsPb_2Br_5$	0.405	75.4	–	43	$\approx 10^{10}$	[122]
	PbS nanoplatelets	0.35–0.65	0.02	–	160	3.96×10^{10}	[156]
	Silicon/BP	1.95	125	–	–	–	[139]
1D	Sb_2Se_3 nanowires	0.52	270	984	<8	1.27×10^{11}	[241]
	V-WO_3 nanorods	0.25–0.9	4.5×10^3	70	2	5.15×10^{11}	[242]
	ZnO:B/Sb_2Se_3 nanorods	0.46	0.137	≈ 40	–	1.33×10^{11}	[189]
	InN/In_2S_3 nanorods	0.365	0.14	–	0.022	4×10^{10}	[33]
	InGaN nanorods	0.385	$\approx 10^5$	10^7	0.05	–	[182]
	GaAsSb	0.532	11.7	2.74×10^3	0.05	1.64×10^{11}	[176]
	PbSe nanorods	0.405–10.64	0.78	–	0.0175	5.1×10^{10}	[185]
	Tellurium nanorods	0.633	6.1	40.9	–	1.2×10^{11}	[243]
	$CsCu_2I_3$	0.265	0.022	10.3	24	1.2×10^{11}	[244]
0D	PbS QDs	0.97	0.46	60	0.49×10^{-3}	2.1×10^{12}	[231]
	PbS QD/MoS_2/WSe_2	0.785	0.76	≈100	0.05	5.15×10^{11}	[110]
	PbS QD/Si	1.28	–	31	0.0025	8.8×10^{10}	[245]
	CdSe QDs	0.36~1.31	8.3×10^3	≈60	90	4.2×10^{17}	[71]
	$CsPbBr_3$ QDs	0.514	0.14	–	12	7.0×10^{11}	[246]
	$CsPbBr_3$ QDs	0.405	10.1	6.4×10^3	–	9.35×10^{13}	[247]
	$CsPbI_3$ QDs	0.450	0.105	–	–	5×10^{13}	[248]
	Si:PbS QDs	1.540	0.264	21.4	0.002	1.47×10^{11}	[249]

artificial visual systems. The integration of optoelectronic synaptic devices also enables the implementation of learning and plasticity functions, which enables artificial neuromorphic visual systems to adapt and improve their visual performance over time. At last, cognitive learning, a process that is crucial for pattern recognition and image/speech processing, is the ability of the memory to recall information based on partial cues. It is achieved through forming connections between the environment and an organism's reactions by experiencing two events together. This creates a link between the internal characteristics of the two events, resulting in the recall of one event when the other is re-experienced.

Optical synaptic devices that can be applied to various wavelength bands are being developed by utilizing the synaptic characteristics of neuromorphic devices. Huang et al. have developed an organic-inorganic QD hybrid infrared heterojunction synaptic phototransistor, which mimics synaptic behavior in response to both NIR and short-wave infrared light (**Figure 9**a).[250] The phototransistor was made of PbS QDs and cross-linked PDPP:C_6Si, and was capable of performing basic biological synaptic functions. The device was also able to perform "AND" and "OR" logic operations using NIR and short-wave infrared light as input signals. A 5 × 5 synaptic array was used to demonstrate image recognition and memory under short-wave infrared light. The phototransistor was also able to adapt to white ambient light and showed strong anti-interference ability. The device was fabricated using a simple solution processing method and could

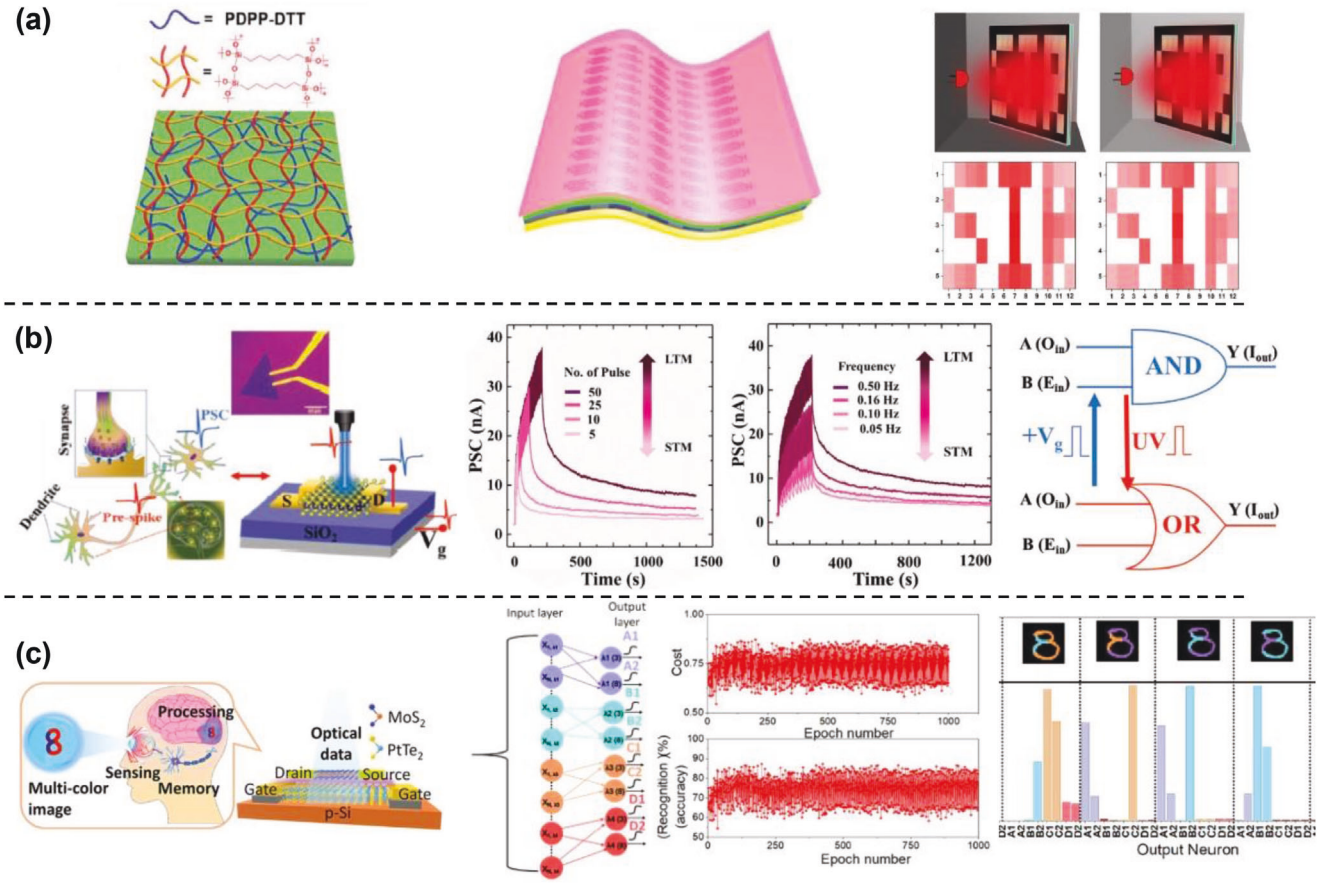

Figure 9. a) Schematic and transfer characteristics of flexible organic/inorganic QD hybrid heterojunction short-wave infrared synaptic phototransistor array and corresponding measured synaptic data. Reproduced with permission.[250] Copyright 2022, Wiley-VCH. b) Comparison of a biological synapse with a proposed MoS_2 artificial synapse, including a device image and response to optical stimulus, as well as the band model of MoS_2 under optical illumination and postsynaptic current for various stimuli. Reproduced with permission.[256] Copyright 2022, Wiley-VCH. c) A neuromorphic optoelectronic synapse device capable of integrating optical sensing, storage, and processing for multi-wavelength pattern recognition. The device employs an ultraviolet–visible MoS_2 field-effect-transistor channel and $PtTe_2$/Si gate electrode to enable short- and long-term potentiation and depression. Reproduced with permission.[259] Copyright 2022, American Chemical Society.

potentially be used in flexible bionic optoelectronic robots for an artificial night vision system. Sahu et al. proposed a 2D MoS_2 optoelectronic artificial synapse that can perform complex neuromorphic behavior, arithmetic operations, and reconfigurable logic gates, which could lead to breakthroughs in non-Von-Neumann in-memory computing architecture for AI applications (Figure 9b).[256] The optoelectronic neuromorphics also implemented reconfigurable Boolean OR and AND gates and basic arithmetic operations, showing the potential of achieving unparalleled heights in 2D for memory neuromorphic computing applications. Islam et al. investigated an optoelectronic synapse device with multifunctional integration of all the processes required for real-time object identification, with a wide range of wavelength sensitivity and artificial neural network training for pattern recognition and object identification (Figure 9c).[259] Also, they developed a single-layer neural network using extracted device parameters for single wavelength and mixed-wavelength pattern recognition tasks. The network was able to identify the target number from the mixed wavelength pattern and recognized the remaining part of the mixed pattern. They utilized the MNIST dataset for training and testing the network and obtained a recognition accuracy of 80% for "3 in 8" patterns. The weight matrix comprised of wavelength-dependent conductance values, which was then utilized to implement vector-matrix multiplication.

3.3. Flexible and Stretchable Optoelectronics

Incorporating flexibility into optoelectronic devices enables them to adapt to different shapes and respond to applied strains, making them suitable for a wide range of intelligent applications.[252,260–262] Despite the rapid advances in organic conductors or semiconductors, the application of flexible PD is still challenging due to their low sensitivity to light irradiation and the need to achieve a balance between electrical and optical properties while maintaining device flexibility.[243,263,247] Recently developed 2D-based semiconductors have shown promising results in terms of their ability to withstand higher levels of strain. In experiments and simulations, these nanomaterials have been demonstrated to endure strains greater than 10%, which is much larger

than the conventional limit of 0.5% to 1.5% for bulk materials. Hence, it is important to consider both the proper materials and optimal design to construct flexible PDs based on nanomaterials for specific environments.[17,228,257,264] Regulating the band structure and optoelectronic properties of a semiconductor through strain modulation is a key strategy to improve device performance. Generally, the photocurrent of a device depends on the generation, separation, transport, and collection of photocarriers. One way to enhance the performance of PD device is to increase the light absorption area by designing a crumpled structure, which leads to the generation of a larger number of photocarriers. Additionally, it has been observed that tensile strain can cause a shift in the absorption spectrum of devices towards the red end and a decrease in bandgap, leading to an improvement in the photocurrent.

Graphene, due to its exceptional mechanical strength among the 2D materials, can significantly enhance the durability and lifespan of a device. A flexible WS_2 PD has been created using multilayer graphene sheets as flexible electrodes and parylene-C as the back-gate insulator.[265] The device demonstrated excellent photoresponse with a high responsivity of 4500 A W^{-1} and fast response time (<2 ms) when the gate voltage was greater than 60 V, due to the tunable graphene electrode contact. Thanks to its superior mechanical properties, output current did not deteriorate significantly under various bending strain conditions, even when wrapped around human skin. Additionally, alloys composed of three elements are of great interest in flexible photodetection due to their continuously tunable bandgaps over a wide range and favorable mechanical properties. Additionally, alloy engineering is seen as a possible solution to reduce localized deep-level defect states, promoting the quick transmission of photogenerated excitons. For example, vapor deposition method has been used to synthesize several non-layered or layered 2D alloys, such as $Pb_{1-x}Sn_xSe$, $CdS_xSe_{(1-x),}$[266] $Sn(S_xSe_{1-x})_2$, $Mo_{0.5}W_{0.5}Se_2$, and SnSSe.[267,110]

Further, flexible materials based optoelectronic devices have been also extensively demonstrated. Nawaz et al. presented a one-step method to fabricate high-performance, flexible PDs based on multicomponent alloyed 1D semiconductors that exhibit broadband absorption and superior spectral photoresponsivity, with several orders of magnitude higher specific detectivity, EQE, rapid response speed, and excellent long-term environmental stability, demonstrating potential for use in optoelectronic devices (**Figure 10**a).[266] Lai et al. proposed the fabrication of high-performance, flexible, and self-powered PDs based on graded rare earth metal halide perovskite phases in a vertical device structure.[268] The PDs showed good performance without any applied voltage, with high responsivity of 444 mA W^{-1} and fast response time of 52 µs. The vertical device structure enhances the mechanical flexibility of rare earth metal halide perovskite as the current flows through metal halide octahedral layers, making the devices more resistant to damage. Kim et al. also demonstrated skin-like ultra-flexible full-color PDs by using monolithic integration of various-sized QDs and IGZO semiconductors (Figure 10b).[71] They introduced trap-reduced chelating chalcometallate ligands for enhancing charge carrier transport between QDs and IGZO as well as fine-patterning of QDs using UV-induced photochemical reaction of the ligands. The ultra-flexible QD PDs were implemented on a skin-like soft platform, which realized biological applications by attaching onto a human fingertip for monitoring of blood oxygen saturation level.

Furthermore, further development of stretchable platform should be considered to enhance mechanical compatibility and exhibit the feasibility of integration of skin-compatible optoelectronics onto human body. Kim et al. have successfully made a stretchable nanolayered BP PD by pre-stressing a polydimethylsiloxane (PDMS) substrate before fabrication.[269] This allowed us to study the effect of uniaxial compression on the optoelectronic properties of BP. The device showed an increase in negative photocurrent generation with compression, which is due to a combination of a reduction in bandgap and a high concentration of oxygenated defects on the BP surface. They provide a general strain engineering approach for 2D materials and potential implications for various devices such as strain-tunable optical sensors and imaging arrays. At last, Kim et al. recently presented high-performance stretchable perovskite PDs using Ag–Au alloy NW-based stretchable electrodes and poly(vinylpyrrolidone)/$MAPbI_3$ composite nanofibers.[270] The resulting devices were able to sustain up to 15% strain, while demonstrating impressive responsivity and detectivity. These highly sensitive, stretchable, and stable PDs have great potential for use in next-generation wearable optical sensor platforms (Figure 10c).

4. Conclusions

Recent researches have made significant progress in the development of PDs based on 2D, 1D, and 0D nanomaterials such as graphene, TMDCs, perovskites, BP, NWs, NRs, NTs, NPs, and QDs. These materials have unique electronic, optical, and mechanical properties that make them promising for use in state-of-the-art PDs. PDs based on graphene, for example, exhibit high photoresponsivity, fast response times, and broad spectral range, making them suitable for various optical sensing applications. In addition, TMDCs have also been widely explored due to their large bandgap and tunable electronic properties. Further, perovskites have attracted attention due to their high absorption coefficient and low defect density. Recent advances have shown several development technologies to produce high-quality and stable nanomaterials, which are tailored in sizes, shapes, and material compositions using various novel synthesis approaches and chemical doping methods, improving charge carrier transfer efficiency and sensitivity with multifunctional properties and multiplexed operations. PDs based on these low-dimensional nanomaterials have been implemented in the photodiode, photoconductor, and phototransistor configurations. The development of flexible and stretchable PDs has also been a significant area of research, where materials such as BP, graphene, and QDs have been integrated with elastic substrates such as PDMS and polyethylene terephthalate. These devices have shown promising results, with high photoresponsivity, fast response times, and high flexibility. Furthermore, more recently, low-dimensional nanomaterials-based PD applications have been extended to realize state-of-the-art optoelectronics such as biosensors, CMOS-compatible devices, and upconversion PDs.

Recent PDs have developed with the above-mentioned advantages, but there are also clearly unresolved limitations such as low responsivity, slow response time, insufficient stability under long-term illumination, and limited spectral range. To overcome

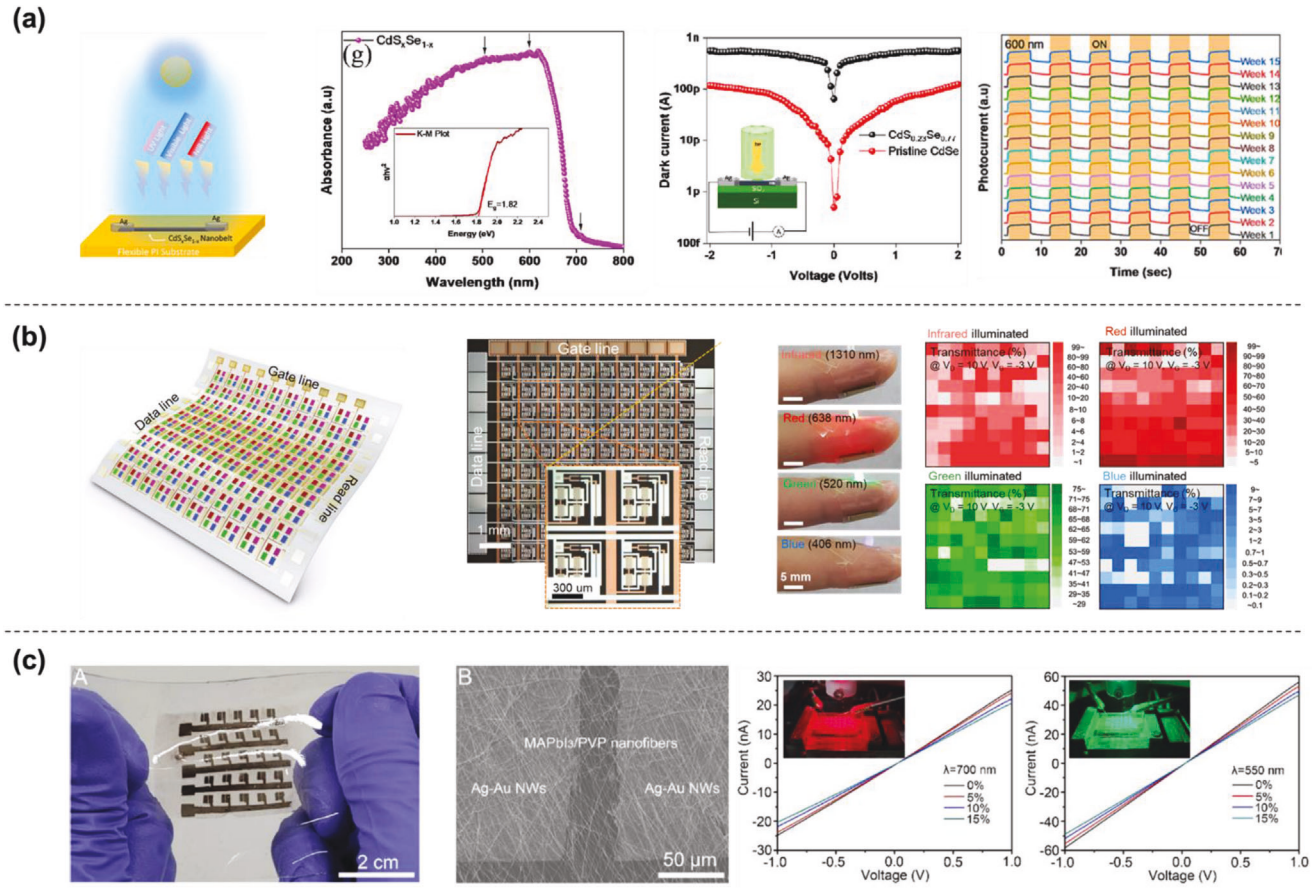

Figure 10. a) High-performance broadband optoelectronics based on low-cost multicomponent alloyed 1D cadmium–sulfur–selenide (CdS_xSe_{1-x}) micro-nanostructures exhibit superior photoresponsivity, detectivity, EQE, and response speed, with long-term environmental stability, and is suitable for flexible optoelectronic devices. Reproduced with permission.[266] Copyright 2022, American Chemical Society. b) A skin-like ultraflexible full-color PD arrays based on QDs and IGZO for bio-imaging applications. Reproduced with permission.[71] Copyright 2019, American Association for Advancement of Science. c) Stretchable photodetectors based on electrospun polymer/perovskite composite nanofibers. Reproduced with permission.[270] Copyright 2022, American Chemical Society.

these limitations, future work is focused on optimizing material selection, device structure, and fabrication process to enhance PD performance. Achieving novel synthesis methods and new designs for high-quality, uniform, and stable nanomaterials are also needed to provide improved photoresponse characteristics of PDs. For practical applications, material growth should be precisely controlled and synthetic yield needs to be increased. Furthermore, there is also ongoing research on incorporating new materials such as perovskites, BPs, and QDs to further expand the spectral range of light absorption. In addition, optimizing heterogeneous structures in terms of directional selection of electronic structure and material properties are very important methods for achieving high device performance and enhancing functionality. Moreover, the development of advanced approach such as laser doping and stress-controlled band structure is also urged to improve charge carrier transfer efficiency and optoelectronic performance of nanoscale PDs. In conclusion, the development of PDs based on nanomaterials such as 2D, 1D, and 0D materials continues to make progress, and new materials, structures, and device configurations are being explored for various photosensing applications. Further, over the past decades, the technical trends of PDs move toward broadband and multi-functional processing with ultrahigh device density and highly integrated device arrays or vertical device architecture. Thus, the fabrication process of nanomaterial-based PDs should be optimized for scalable system-level integration with enhanced device performance, stability, and uniformity as well as ultimate processing speed and energy efficiency. In particular, the integration of flexible and stretchable materials is a promising area for future work as it has the potential to lead to new applications in wearable technology and flexible optoelectronic devices.

Acknowledgements

J.K. and J.L. contributed equally to this work. This research was partially supported by the National Research Foundation of Korea (NRF) grant funded by the Korea government (MSIP) (No. NRF-2019R1A2C2002447) and by the Engineering Research Center of Excellence (ERC) Program supported by National Research Foundation (NRF), Korean Ministry of Science & ICT (MSIT) (Grant No. NRF-2017R1A5A1014708). J.K., A.F. and T.J.M. acknowledge the support of the AFOSR (contract # FA9550-22-1-0423), the U.S. Office of Naval Research Contract # N00014-20-1-2116 by the U.S. Department of Commerce, National Institute of Standards and

Technology as part of the Center for Hierarchical Materials Design Award #70NANB10H005, BSF (award # 2020384), NSF (DMR-2223922).

Conflict of Interest

The authors declare no conflict of interest.

Keywords

nanomaterials, optoelectronics, photodetectors, photonic devices

Received: February 25, 2023
Revised: April 21, 2023
Published online:

[1] S. Watson, W. Zhang, J. Tavares, J. Figueiredo, H. Cantu, J. Wang, E. Wasige, H. Salgado, L. Pessoa, A. Kelly, *Microwave Opt. Technol. Lett.* **2019**, *61*, 1121.
[2] A. Pospischil, M. Humer, M. M. Furchi, D. Bachmann, R. Guider, T. Fromherz, T. Mueller, *Nat. Photonics* **2013**, *7*, 892.
[3] J. Liu, J. Jiang, S. Wang, T. Li, X. Jing, Y. Liu, Y. Wang, H. Wen, M. Yao, X. Zhan, L. Shen, *Small* **2021**, *17*, e2101316.
[4] S.-E. Ahn, I. Song, S. Jeon, Y. W. Jeon, Y. Kim, C. Kim, B. Ryu, J.-H. Lee, A. Nathan, S. Lee, G. T. Kim, U.-I. Chung, *Adv. Mater.* **2012**, *24*, 2631.
[5] X. Xu, J. Chen, S. Cai, Z. Long, Y. Zhang, L. Su, S. He, C. Tang, P. Liu, H. Peng, X. Fang, *Adv. Mater.* **2018**, *30*, 1803165.
[6] Z. Li, M. K. Joshi, J. Chen, Z. Zhang, Z. Li, X. Fang, *Adv. Funct. Mater.* **2020**, *30*, 2005291.
[7] A. Bablich, M. Müller, P. Kienitz, R. Bornemann, C. O. Ogolla, B. Butz, B. Choubey, P. H. Bolívar, *Sci. Rep.* **2022**, *12*, 10178.
[8] Z. Ji, G. Cen, C. Su, Y. Liu, Z. Zhao, C. Zhao, W. Mai, *Adv. Opt. Mater.* **2020**, *8*, 2001436.
[9] C. Hung, Y. Chiang, Y. Lin, Y. Chiu, W. Chen, *Adv. Sci.* **2021**, *8*, 2100742.
[10] H. Xu, J. Liu, J. Zhang, G. Zhou, N. Luo, N. Zhao, *Adv. Mater.* **2017**, *29*, 1700975.
[11] C. M. Lochner, Y. Khan, A. Pierre, A. C. Arias, *Nat. Commun.* **2014**, *5*, 5745.
[12] A. Glushkova, P. Andričević, R. Smajda, B. Náfrádi, M. Kollár, V. Djokić, A. Arakcheeva, L. Forró, R. Pugin, E. Horváth, *ACS Nano* **2021**, *15*, 4077.
[13] D. Vikraman, H. Liu, S. Hussain, S. H. A. Jaffery, K. Karuppasamy, E. Jo, Z. Abbas, J. Jung, J. Kang, H. Kim, *Small* **2022**, *18*, 2104216.
[14] C. Zhao, Z. He, P. Wangyang, J. Tan, C. Shi, A. Pan, L. He, Y. Liu, *ACS Appl. Nano Mater.* **2022**, *5*, 13737.
[15] J. Chen, W. Ouyang, W. Yang, J. He, X. Fang, *Adv. Funct. Mater.* **2020**, *30*, 1909909.
[16] J. He, P. Xu, R. Zhou, H. Li, H. Zu, J. Zhang, Y. Qin, X. Liu, F. Wang, *Adv. Electron. Mater.* **2022**, *8*, 2100997.
[17] Y. Peng, J. Lu, X. Wang, W. Ma, M. Que, Q. Chen, F. Li, X. Liu, W. Gao, C. Pan, *Nano Energy* **2022**, *94*, 106945.
[18] A. Costas, C. Florica, N. Preda, C. Besleaga, A. Kuncser, I. Enculescu, *Sci. Rep.* **2022**, *12*, 6834.
[19] M.-S. Jo, H.-J. Song, B.-J. Kim, Y.-K. Shin, S.-H. Kim, X. Tian, S.-M. Kim, M.-H. Seo, J.-B. Yoon, *Sci. Rep.* **2022**, *12*, 2284.
[20] V. Adepu, A. Kunchur, C. S. R. Kolli, S. Siddhartha, V. Mattela, P. Sahatiya, *ACS Appl. Nano Mater.* **2022**, *5*, 6852.
[21] Z. Liu, X. Jia, W. Duan, X. Zhu, B. He, C. Sun, M. Wang, E. Li, C. Fan, *Adv. Opt. Mater.* **2023**, *11*, 2202087.
[22] W. Pan, M. Tan, Y. He, H. Wei, B. Yang, *Nano Lett.* **2022**, *22*, 2277.
[23] L. Mei, R. Huang, C. Shen, J. Hu, P. Wang, Z. Xu, Z. Huang, L. Zhu, *Adv. Opt. Mater.* **2022**, *10*, 2102656.
[24] S. Huang, Q. Wu, Z. Jia, X. Jin, X. Fu, H. Huang, X. Zhang, J. Yao, J. Xu, *Adv. Opt. Mater.* **2020**, *8*, 1901808.
[25] S. Lara-Avila, A. Danilov, D. Golubev, H. He, K. H. Kim, R. Yakimova, F. Lombardi, T. Bauch, S. Cherednichenko, S. Kubatkin, *Nat. Astron.* **2019**, *3*, 983.
[26] K. Jani, D. Shoemaker, C. Cutler, *Nat. Astron.* **2020**, *4*, 260.
[27] A. Xomalis, X. Zheng, R. Chikkaraddy, Z. Koczor-Benda, E. Miele, E. Rosta, G. A. E. Vandenbosch, A. Martínez, J. J. Baumberg, *Science* **2021**, *374*, 1268.
[28] S. Yanikgonul, V. Leong, J. R. Ong, T. Hu, S. Y. Siew, C. E. Png, L. Krivitsky, *Nat. Commun.* **2021**, *12*, 1834.
[29] W. Yang, J. Chen, Y. Zhang, Y. Zhang, J. He, X. Fang, *Adv. Funct. Mater.* **2019**, *29*, 1808182.
[30] W. Tian, D. Liu, F. Cao, L. Li, *Adv. Opt. Mater.* **2017**, *5*, 1600468.
[31] H.-P. Wang, S. Li, X. Liu, Z. Shi, X. Fang, J.-H. He, *Adv. Mater.* **2021**, *33*, 2003309.
[32] M. Kim, G. Bae, K. N. Kim, H. Jo, D. S. Song, S. Ji, D. Jeon, S. Ko, S. J. Lee, S. Choi, S. Yim, W. Song, S. Myung, D. H. Yoon, K.-S. An, S. S. Lee, *NPG Asia Mater.* **2022**, *14*, 89.
[33] B. Cao, Q. Liu, Y. Zheng, X. Tang, J. Chai, S. Ma, W. Wang, G. Li, *Adv. Funct. Mater.* **2022**, *32*, 2110715.
[34] Y. Zhang, M. Vafaie, J. Xu, J. M. Pina, P. Xia, A. M. Najarian, O. Atan, M. Imran, K. Xie, S. Hoogland, E. H. Sargent, *Adv. Mater.* **2022**, *34*, 2206884.
[35] R. Guo, M. Zhang, J. Ding, A. Liu, F. Huang, M. Sheng, *J. Mater. Chem. C* **2022**, *10*, 7404.
[36] X. Wei, S. Li, W. Wang, X. Zhang, W. Zhou, S. Xie, H. Liu, *Adv. Sci.* **2022**, *9*, 2200054.
[37] M. Zhao, Y. Hao, C. Zhang, R. Zhai, B. Liu, W. Liu, C. Wang, S. H. M. Jafri, A. Razaq, R. Papadakis, J. Liu, X. Ye, X. Zheng, H. Li, *Crystals* **2022**, *12*, 1087.
[38] C. Gong, K. Hu, X. Wang, P. Wangyang, C. Yan, J. Chu, M. Liao, L. Dai, T. Zhai, C. Wang, L. Li, J. Xiong, *Adv. Funct. Mater.* **2018**, *28*, 1706559.
[39] D. Jariwala, V. K. Sangwan, L. J. Lauhon, T. J. Marks, M. C. Hersam, *Chem. Soc. Rev.* **2013**, *42*, 2824.
[40] N. Huo, G. Konstantatos, *Adv. Mater.* **2018**, *30*, 1801164.
[41] S. Sagadevan, M. M. Shahid, Z. Yiqiang, W.-C. Oh, T. Soga, J. Anita Lett, S. F. Alshahateet, I. Fatimah, A. Waqar, S. Paiman, M. R. Johan, *Nanotechnol. Rev.* **2021**, *10*, 605.
[42] F. Zhang, K. Yang, G. Liu, Y. Chen, M. Wang, S. Li, R. Li, *Composites, Part A* **2022**, *160*, 107051.
[43] Z. Hu, Y. Zhao, W. Zou, Q. Lu, J. Liao, F. Li, M. Shang, L. Lin, Z. Liu, *Adv. Funct. Mater.* **2022**, *32*, 2203179.
[44] Q. H. Wang, K. Kalantar-Zadeh, A. Kis, J. N. Coleman, M. S. Strano, *Nat. Nanotechnol.* **2012**, *7*, 699.
[45] H. Tian, M. L. Chin, S. Najmaei, Q. Guo, F. Xia, H. Wang, M. Dubey, *Nano Res.* **2016**, *9*, 1543.
[46] K. F. Mak, J. Shan, *Nat. Photonics* **2016**, *10*, 216.
[47] A. A. Tedstone, D. J. Lewis, P. O'Brien, *Chem. Mater.* **2016**, *28*, 1965.
[48] Z. Ren, *Mater. Today Phys.* **2017**, *1*, 2.
[49] Y. Wang, L. Zhou, M. Zhong, Y. Liu, S. Xiao, J. He, *Nano Res.* **2022**, *15*, 3675.
[50] S. A. Han, R. Bhatia, S.-W. Kim, *Nano Convergence* **2015**, *2*, 17.
[51] C. Gong, Y. Zhang, W. Chen, J. Chu, T. Lei, J. Pu, L. Dai, C. Wu, Y. Cheng, T. Zhai, L. Li, J. Xiong, *Adv. Sci.* **2017**, *4*, 1700231.
[52] S. Chen, G. Shi, *Adv. Mater.* **2017**, *29*, 1605448.
[53] Y. Zhang, C. K. Lim, Z. Dai, G. Yu, J. W. Haus, H. Zhang, P. N. Prasad, *Phys. Rep.* **2019**, *795*, 1.
[54] H. Li, T. Luo, S. Zhang, Z. Sun, X. He, W. Zhang, H. Chang, *Energy Environ. Mater.* **2021**, *4*, 46.

[55] T. Song, Q.-X. Ma, Q. Wang, H.-L. Zhang, *Mater. Adv.* **2022**, *3*, 756.
[56] Y. Yi, X. F. Yu, W. Zhou, J. Wang, P. K. Chu, *Mater. Sci. Eng., R.* **2017**, *120*, 1.
[57] P. C. Debnath, K. Park, Y. W. Song, *Small Methods* **2018**, *2*, 1700315.
[58] K. S. Novoselov, A. K. Geim, S. V. Morozov, D. Jiang, Y. Zhang, S. V. Dubonos, I. V. Grigorieva, A. A. Firsov, *Science* **2004**, *306*, 666.
[59] Y.-Y. Li, B. Gao, Y. Han, B.-K. Chen, J.-Y. Huo, *Front. Phys.* **2021**, *16*, 43301.
[60] Y. Zhang, J. Wu, M. Aagesen, H. Liu, *J. Phys. D: Appl. Phys.* **2015**, *48*, 463001.
[61] L. N. Quan, J. Kang, C.-Z. Ning, P. Yang, *Chem. Rev.* **2019**, *119*, 9153.
[62] S. L. Choon, H. N. Lim, I. Ibrahim, Z. Zainal, K. B. Tan, C. Y. Foo, C. H. Ng, *Renewable Sustainable Energy Rev.* **2023**, *171*, 113037.
[63] S. Nanot, E. H. Hároz, J.-H. Kim, R. H. Hauge, J. Kono, *Adv. Mater.* **2012**, *24*, 4977.
[64] S. Aftab, M. Z. Iqbal, Y. S. Rim, *Small* **2023**, *19*, 2205418.
[65] A. P. Litvin, X. Zhang, E. v. Ushakova, A. L. Rogach, *Adv. Funct. Mater.* **2021**, *31*, 2010768.
[66] J. Y. Kim, O. Voznyy, D. Zhitomirsky, E. H. Sargent, *Adv. Mater.* **2013**, *25*, 4986.
[67] D. Ghosh, K. Sarkar, P. Devi, K.-H. Kim, P. Kumar, *Renewable Sustainable Energy Rev.* **2021**, *135*, 110391.
[68] S. Miao, Y. Cho, *Front. Energy Res.* **2021**, *9*, 666534.
[69] L. Li, G. Wu, G. Yang, J. Peng, J. Zhao, J.-J. Zhu, *Nanoscale* **2013**, *5*, 4015.
[70] D. K. Hwang, Y. T. Lee, H. S. Lee, Y. J. Lee, S. H. Shokouh, J. Kyhm, J. Lee, H. H. Kim, T.-H. Yoo, S. H. Nam, D. I. Son, B.-K. Ju, M.-C. Park, J. D. Song, W. K. Choi, S. Im, *NPG Asia Mater.* **2016**, *8*, e233.
[71] J. Kim, S.-M. Kwon, Y. K. Kang, Y.-H. Kim, M.-J. Lee, K. Han, A. Facchetti, M.-G. Kim, S. K. Park, *Sci. Adv.* **2019**, *5*, eaax8801.
[72] J. Kim, C. Jo, M. Kim, G. Park, T. J. Marks, A. Facchetti, S. K. Park, *Adv. Mater.* **2022**, *34*, 2106215.
[73] J. Kim, S. Song, Y.-H. Kim, S. K. Park, *Small Struct.* **2021**, *2*, 2000024.
[74] L. Li, C. Hu, G. Shen, *Acc Mater. Res.* **2021**, *2*, 954.
[75] H. Chang, H. Wu, *Adv. Funct. Mater.* **2013**, *23*, 1984.
[76] J. R. Prekodravac, D. P. Kepić, J. C. Colmenares, D. A. Giannakoudakis, S. P. Jovanović, *J. Mater. Chem. C* **2021**, *9*, 6722.
[77] N. Kumar, R. Salehiyan, V. Chauke, O. Joseph Botlhoko, K. Setshedi, M. Scriba, M. Masukume, S. Sinha Ray, *FlatChem* **2021**, *27*, 100224.
[78] B. Sun, J. Pang, Q. Cheng, S. Zhang, Y. Li, C. Zhang, D. Sun, B. Ibarlucea, Y. Li, D. Chen, H. Fan, Q. Han, M. Chao, H. Liu, J. Wang, G. Cuniberti, L. Han, W. Zhou, *Adv. Mater. Technol.* **2021**, *6*, 2000744.
[79] J. Du, B. Tong, S. Yuan, N. Dai, R. Liu, D. Zhang, H. Cheng, W. Ren, *Adv. Funct. Mater.* **2022**, *32*, 2203115.
[80] F. Xia, T. Mueller, Y. Lin, A. Valdes-Garcia, P. Avouris, *Nat. Nanotechnol.* **2009**, *4*, 839.
[81] X. Gan, R.-J. Shiue, Y. Gao, I. Meric, T. F. Heinz, K. Shepard, J. Hone, S. Assefa, D. Englund, *Nat. Photonics* **2013**, *7*, 883.
[82] B. Y. Zhang, T. Liu, B. Meng, X. Li, G. Liang, X. Hu, Q. J. Wang, *Nat. Commun.* **2013**, *4*, 1811.
[83] H. Jiang, J. Wei, F. Sun, C. Nie, J. Fu, H. Shi, J. Sun, X. Wei, C.-W. Qiu, *ACS Nano* **2022**, *16*, 4458.
[84] U. Sassi, R. Parret, S. Nanot, M. Bruna, S. Borini, D. de Fazio, Z. Zhao, E. Lidorikis, F. H. L. Koppens, A. C. Ferrari, A. Colli, *Nat. Commun.* **2017**, *8*, 14311.
[85] M. W. Shabbir, M. N. Leuenberger, *ACS Nano* **2022**, *16*, 5529.
[86] W. Zhang, H. Xu, F. Xie, X. Ma, B. Niu, M. Chen, H. Zhang, Y. Zhang, D. Long, *Nat. Commun.* **2022**, *13*, 471.
[87] Z. Huang, J. Liu, T. Zhang, Y. Jin, J. Wang, S. Fan, Q. Li, *ACS Appl. Mater. Interfaces* **2021**, *13*, 22796.
[88] V. X. Ho, Y. Wang, L. Howe, M. P. Cooney, N. Q. Vinh, *ACS Appl. Nano Mater.* **2022**, *5*, 12477.
[89] M. Peng, Y. Yu, Z. Wang, X. Fu, Y. Gu, Y. Wang, K. Zhang, Z. Zhang, M. Huang, Z. Cui, F. Zhong, P. Wu, J. Ye, T. Xu, Q. Li, P. Wang, F. Yue, F. Wu, J. Dai, C. Chen, W. Hu, *ACS Photonics* **2022**, *9*, 1775.
[90] X. Chen, X. Liu, B. Wu, H. Nan, H. Guo, Z. Ni, F. Wang, X. Wang, Y. Shi, X. Wang, *Nano Lett.* **2017**, *17*, 6391.
[91] J. Han, J. Wang, M. Yang, X. Kong, X. Chen, Z. Huang, H. Guo, J. Gou, S. Tao, Z. Liu, Z. Wu, Y. Jiang, X. Wang, *Adv. Mater.* **2018**, *30*, 1804020.
[92] W. Liu, J. Lv, L. Peng, H. Guo, C. Liu, Y. Liu, W. Li, L. Li, L. Liu, P. Wang, S. C. Bodepudi, K. Shehzad, G. Hu, K. Liu, Z. Sun, T. Hasan, Y. Xu, X. Wang, C. Gao, B. Yu, X. Duan, *Nat. Electron.* **2022**, *5*, 281.
[93] A. K. Singh, P. Kumar, D. J. Late, A. Kumar, S. Patel, J. Singh, *Appl. Mater. Today* **2018**, *13*, 242.
[94] U. Krishnan, M. Kaur, K. Singh, M. Kumar, A. Kumar, *Superlattices Microstruct.* **2019**, *128*, 274.
[95] H. Xu, J. Zhu, Q. Ma, J. Ma, H. Bai, L. Chen, S. Mu, *Micromachines* **2021**, *12*, 240.
[96] T. Nawz, A. Safdar, M. Hussain, D. Sung Lee, M. Siyar, *Crystals* **2020**, *10*, 902.
[97] M. Wu, Y. Xiao, Y. Zeng, Y. Zhou, X. Zeng, L. Zhang, W. Liao, *InfoMat* **2021**, *3*, 362.
[98] S. Rani, M. Sharma, D. Verma, A. Ghanghass, R. Bhatia, I. Sameera, *Mater. Sci. Semicond. Process.* **2022**, *139*, 106313.
[99] Y. Shi, H. Li, L.-J. Li, *Chem. Soc. Rev.* **2015**, *44*, 2744.
[100] J. You, M. D. Hossain, Z. Luo, *Nano Convergence* **2018**, *5*, 26.
[101] Y. Yu, C. Li, Y. Liu, L. Su, Y. Zhang, L. Cao, *Sci. Rep.* **2013**, *3*, 1866.
[102] Q. Zhang, H. Ying, X. Li, R. Xiang, Y. Zheng, H. Wang, J. Su, M. Xu, X. Zheng, S. Maruyama, X. Zhang, *ACS Appl. Mater. Interfaces* **2021**, *13*, 31861.
[103] Q. Zeng, Z. Liu, *Adv. Electron. Mater.* **2018**, *4*, 1700335.
[104] Q. Lv, R. Lv, *Carbon* **2019**, *145*, 240.
[105] J. Li, E. Liu, Y. Ma, X. Hu, J. Wan, L. Sun, J. Fan, *Appl. Surf. Sci.* **2016**, *364*, 694.
[106] F. Chen, L. Wang, X. Ji, Q. Zhang, *ACS Appl. Mater. Interfaces* **2017**, *9*, 30821.
[107] P. K. Sahoo, S. Memaran, F. A. Nugera, Y. Xin, T. Díaz Márquez, Z. Lu, W. Zheng, N. D. Zhigadlo, D. Smirnov, L. Balicas, H. R. Gutiérrez, *ACS Nano* **2019**, *13*, 12372.
[108] E. Najafidehaghani, Z. Gan, A. George, T. Lehnert, G. Q. Ngo, C. Neumann, T. Bucher, I. Staude, D. Kaiser, T. Vogl, U. Hübner, U. Kaiser, F. Eilenberger, A. Turchanin, *Adv. Funct. Mater.* **2021**, *31*, 2101086.
[109] X. Wang, L. Pan, J. Yang, B. Li, Y. Liu, Z. Wei, *Adv. Mater.* **2021**, *33*, 2006908.
[110] P. Zeng, W. Wang, D. Han, J. Zhang, Z. Yu, J. He, P. Zheng, H. Zheng, L. Zheng, W. Su, D. Huo, Z. Ni, Y. Zhang, Z. Wu, *ACS Nano* **2022**, *16*, 9329.
[111] S. Mukherjee, D. Bhattacharya, S. K. Ray, A. N. Pal, *ACS Appl. Mater. Interfaces* **2022**, *14*, 34875.
[112] A. Dodda, D. Jayachandran, A. Pannone, N. Trainor, S. P. Stepanoff, M. A. Steves, S. S. Radhakrishnan, S. Bachu, C. W. Ordonez, J. R. Shallenberger, J. M. Redwing, K. L. Knappenberger, D. E. Wolfe, S. Das, *Nat. Mater.* **2022**, *21*, 1379.
[113] J.-C. Blancon, J. Even, C. C. Stoumpos, M. G. Kanatzidis, A. D. Mohite, *Nat. Nanotechnol.* **2020**, *15*, 969.
[114] W. Guo, Z. Yang, J. Dang, M. Wang, *Nano Energy* **2021**, *86*, 106129.
[115] S.-Q. Luo, J.-F. Wang, B. Yang, Y.-B. Yuan, *Front. Phys.* **2019**, *14*, 53401.
[116] X. Sheng, Y. Li, M. Xia, E. Shi, *J. Mater. Chem. A* **2022**, *10*, 19169.
[117] Z. Tan, Y. Wu, H. Hong, J. Yin, J. Zhang, L. Lin, M. Wang, X. Sun, L. Sun, Y. Huang, K. Liu, Z. Liu, H. Peng, *J. Am. Chem. Soc.* **2016**, *138*, 16612.
[118] J. Jagielski, S. Kumar, W.-Y. Yu, C.-J. Shih, *J. Mater. Chem. C* **2017**, *5*, 5610.

[119] H. Wang, J. Ma, D. Li, *J. Phys. Chem. Lett.* **2021**, *12*, 8178.
[120] Y.-T. Li, L. Han, H. Liu, K. Sun, D. Luo, X.-L. Guo, D.-L. Yu, T.-L. Ren, *ACS Appl. Electron. Mater.* **2022**, *4*, 547.
[121] S. Li, Y. Zhang, W. Yang, H. Liu, X. Fang, *Adv. Mater.* **2020**, *32*, 1905443.
[122] R. Wang, Z. Li, S. Li, P. Wang, J. Xiu, G. Wei, H. Liu, N. Jiang, Y. Liu, M. Zhong, *ACS Appl. Mater. Interfaces* **2020**, *12*, 41919.
[123] K.-L. Chu, C.-H. Chen, S.-W. Shen, C.-Y. Huang, Y.-X. Chou, M.-Y. Liao, M.-L. Tsai, C.-I. Wu, C.-C. Chueh, *Chem. Eng. J.* **2021**, *422*, 130112.
[124] R. Sun, D. Zhou, P. Lu, X. Jing, X. Zhuang, S. Liu, Y. Wang, X. Bai, W. Xu, H. Song, *Nano Energy* **2022**, *93*, 106815.
[125] J. Lv, X. Lu, X. Li, M. Xu, J. Zhong, X. Zheng, Y. Shi, X. Zhang, Q. Zhang, *Small* **2022**, *18*, 2201715.
[126] J. Liu, Y. Xue, Z. Wang, Z.-Q. Xu, C. Zheng, B. Weber, J. Song, Y. Wang, Y. Lu, Y. Zhang, Q. Bao, *ACS Nano* **2016**, *10*, 3536.
[127] J. Ma, C. Fang, C. Chen, L. Jin, J. Wang, S. Wang, J. Tang, D. Li, *ACS Nano* **2019**, *13*, 3659.
[128] C.-H. Lin, B. Cheng, T.-Y. Li, J. R. D. Retamal, T.-C. Wei, H.-C. Fu, X. Fang, J.-H. He, *ACS Nano* **2018**, *13*, 1168.
[129] T. Yang, X. Wang, B. Zheng, Z. Qi, C. Ma, Y. Fu, Y. Fu, M. P. Hautzinger, Y. Jiang, Z. Li, P. Fan, F. Li, W. Zheng, Z. Luo, J. Liu, B. Yang, S. Chen, D. Li, L. Zhang, S. Jin, A. Pan, *ACS Nano* **2019**, *13*, 7996.
[130] R. F. Hossain, M. Min, L.-C. Ma, S. R. Sakri, A. B. Kaul, *npj 2D Mater. Appl.* **2021**, *5*, 34.
[131] F. Xia, H. Wang, Y. Jia, *Nat. Commun.* **2014**, *5*, 4458.
[132] V. Eswaraiah, Q. Zeng, Y. Long, Z. Liu, *Small* **2016**, *12*, 3480.
[133] S. H. Aldave, M. N. Yogeesh, W. Zhu, J. Kim, S. S. Sonde, A. P. Nayak, D. Akinwande, *2D Mater.* **2016**, *3*, 014007.
[134] L. Li, Y. Yu, G. J. Ye, Q. Ge, X. Ou, H. Wu, D. Feng, X. H. Chen, Y. Zhang, *Nat. Nanotechnol.* **2014**, *9*, 372.
[135] A. Castellanos-Gomez, L. Vicarelli, E. Prada, J. O. Island, K. L. Narasimha-Acharya, S. I. Blanter, D. J. Groenendijk, M. Buscema, G. A. Steele, J. v Alvarez, H. W. Zandbergen, J. J. Palacios, H. S. J. van der Zant, *2D Mater.* **2014**, *1*, 025001.
[136] P. Chen, N. Li, X. Chen, W.-J. Ong, X. Zhao, *2D Mater.* **2017**, *5*, 014002.
[137] K. Wang, Z. He, X. Li, K. Xu, Q. Zhou, X. Ye, T. Zhang, S. Jiang, Y. Zhang, B. Hu, C. Chen, *Nano Res.* **2023**, *16*, 1651.
[138] Y. Xu, X. Shi, Y. Zhang, H. Zhang, Q. Zhang, Z. Huang, X. Xu, J. Guo, H. Zhang, L. Sun, Z. Zeng, A. Pan, K. Zhang, *Nat. Commun.* **2020**, *11*, 1330.
[139] C. Liu, J. Guo, L. Yu, Y. Xiang, H. Xiang, J. Li, D. Dai, *ACS Photonics* **2022**, *9*, 1764.
[140] S. Thurakkal, X. Zhang, *Mater. Chem. Front.* **2021**, *5*, 2824.
[141] D. J. Perello, S. H. Chae, S. Song, Y. H. Lee, *Nat. Commun.* **2015**, *6*, 7809.
[142] L. Zhang, B. Wang, Y. Zhou, C. Wang, X. Chen, H. Zhang, *Adv. Opt. Mater.* **2020**, *8*, 2000045.
[143] M. Kaur, H. Tyagi, A. Kundu, B. Kaur, M. Raturi, J. Saini, K. S. Hazra, *Adv. Mater. Interfaces* **2022**, *9*, 2201320.
[144] V. Krishnamurthi, M. X. Low, S. Kuriakose, S. Sriram, M. Bhaskaran, S. Walia, *ACS Appl. Nano Mater.* **2021**, *4*, 6928.
[145] Y. Chen, C. Tan, Z. Wang, J. Miao, X. Ge, T. Zhao, K. Liao, H. Ge, Y. Wang, F. Wang, Y. Zhou, P. Wang, X. Zhou, C. Shan, H. Peng, W. Hu, *Sci. Adv.* **2022**, *8*, 1781.
[146] D. Li, R. Li, D. Zhou, F. Zeng, X. Qin, W. Yan, S. Cai, *Appl. Surf. Sci.* **2023**, *609*, 155032.
[147] J. An, X. Zhao, Y. Zhang, M. Liu, J. Yuan, X. Sun, Z. Zhang, B. Wang, S. Li, D. Li, *Adv. Funct. Mater.* **2022**, *32*, 2110119.
[148] X. Zhuang, Y. Mai, D. Wu, F. Zhang, X. Feng, *Adv. Mater.* **2015**, *27*, 403.
[149] W. Zhang, Q. Wang, Y. Chen, Z. Wang, A. T. S. Wee, *2D Mater.* **2016**, *3*, 022001.
[150] X. Hu, K. Liu, Y. Cai, S.-Q. Zang, T. Zhai, *Small Sci.* **2022**, *2*, 2200008.
[151] T. Alkathiri, K. Xu, B. Y. Zhang, M. W. Khan, A. Jannat, N. Syed, A. F. M. Almutairi, N. Ha, M. M. Y. A. Alsaif, N. Pillai, Z. Li, T. Daeneke, J. Z. Ou, *Small Sci.* **2022**, *2*, 2100097.
[152] Z. Liu, J. Liu, P. Yin, Y. Ge, O. A. Al-Hartomy, A. Al-Ghamdi, S. Wageh, Y. Tang, H. Zhang, *Adv. Funct. Mater.* **2022**, *32*, 2206507.
[153] S. Yadav, M. A. Sadique, A. Kaushik, P. Ranjan, R. Khan, A. K. Srivastava, *J. Mater. Chem. B* **2022**, *10*, 1146.
[154] Y.-L. Hong, Z. Liu, L. Wang, T. Zhou, W. Ma, C. Xu, S. Feng, L. Chen, M.-L. Chen, D.-M. Sun, X.-Q. Chen, H.-M. Cheng, W. Ren, *Science* **2020**, *369*, 670.
[155] I. J. Echols, J. Yun, H. Cao, R. M. Thakur, A. Sarmah, Z. Tan, R. Littleton, M. Radovic, M. J. Green, J. L. Lutkenhaus, *Chem. Mater.* **2022**, *34*, 4884.
[156] L. Gao, H. Chen, R. Wang, S. Wei, A. v. Kuklin, S. Mei, F. Zhang, Y. Zhang, X. Jiang, Z. Luo, S. Xu, H. Zhang, H. Ågren, *Small* **2021**, *17*, 2005913.
[157] X. Guo, Y. Wang, A. Elbourne, A. Mazumder, C. K. Nguyen, V. Krishnamurthi, J. Yu, P. C. Sherrell, T. Daeneke, S. Walia, Y. Li, A. Zavabeti, *Nanoscale* **2022**, *14*, 6802.
[158] Y. Peng, Q. Zhu, W. Xu, J. Cao, *ACS Appl. Mater. Interfaces* **2022**, *14*, 27056.
[159] S. Bahti, M. Kibbou, N. Khossossi, I. Essaoudi, A. Ainane, R. Ahuja, *Phys. E* **2022**, *142*, 115229.
[160] H. Deng, D. Dong, K. Qiao, L. Bu, B. Li, D. Yang, H.-E. Wang, Y. Cheng, Z. Zhao, J. Tang, H. Song, *Nanoscale* **2015**, *7*, 4163.
[161] S. Zhuo, J. Zhang, Y. Shi, Y. Huang, B. Zhang, *Angew. Chem.* **2015**, *127*, 5785.
[162] Y. Zhou, J. Luo, Y. Zhao, C. Ge, C. Wang, L. Gao, C. Zhang, M. Hu, G. Niu, J. Tang, *Adv. Opt. Mater.* **2018**, *6*, 1800679.
[163] Q. Lv, X. Wang, L. Liao, *Adv. Funct. Mater.* **2022**, *32*, 2202364.
[164] X. Liu, S. Liu, L. Y. Antipina, Y. Zhu, J. Ning, J. Liu, C. Yue, A. Joshy, Y. Zhu, J. Sun, A. M. Sanchez, P. B. Sorokin, Z. Mao, Q. Xiong, J. Wei, *Nano Res.* **2020**, *13*, 1627.
[165] E. Sutter, J. S. French, S. Sutter, J. C. Idrobo, P. Sutter, *ACS Nano* **2020**, *14*, 6117.
[166] Y. Kumaresan, G. Min, A. S. Dahiya, A. Ejaz, D. Shakthivel, R. Dahiya, *Adv. Mater. Technol.* **2022**, *7*, 2100804.
[167] P. Xie, Y. Huang, W. Wang, Y. Meng, Z. Lai, F. Wang, S. P. Yip, X. Bu, W. Wang, D. Li, J. Sun, J. C. Ho, *Nano Energy* **2022**, *91*, 106654.
[168] Y. Wang, X. Liu, Q. He, G. Chen, D. Xu, X. Chen, W. Zhao, J. Bao, X. Xu, J. Liu, X. Wang, *Adv. Funct. Mater.* **2021**, *31*, 2011251.
[169] G. S. Kumar, R. R. Sumukam, R. K. Rajaboina, R. N. Savu, M. Srinivas, M. Banavoth, *ACS Appl. Energy Mater.* **2022**, *5*, 1342.
[170] D. Zhang, Q. Zhang, Y. Zhu, S. Poddar, Y. Zhang, L. Gu, H. Zeng, Z. Fan, *Adv. Energy Mater.* **2022**, https://doi.org/10.1002/aenm.202201735.
[171] Y. Fu, H. Zhu, J. Chen, M. P. Hautzinger, X. Y. Zhu, S. Jin, *Nat. Rev. Mater.* **2019**, *4*, 169.
[172] H. Anabestani, R. Shazzad, M. F. al Fattah, J. Therrien, D. Ban, *Mater. Today Commun.* **2021**, *28*, 102542.
[173] K. Zhao, J. Yang, M. Zhong, Q. Gao, Y. Wang, X. Wang, W. Shen, C. Hu, K. Wang, G. Shen, M. Li, J. Wang, W. Hu, Z. Wei, *Adv. Funct. Mater.* **2021**, *31*, 2006601.
[174] X. Li, Y. Zhang, L. Zhai, C. Tao, D. Xu, Z. Mu, M. Ding, X. Wu, *Angew. Chem.* **2021**, *133*, 3517.
[175] K. H. Choi, B. J. Jeong, J. Jeon, Y. K. Chung, D. Sung, S. O. Yoon, S. Chae, B. J. Kim, S. Oh, S. H. Lee, C. Woo, X. Dong, A. Ghulam, J. Ali, T. Y. Kim, M. Seo, J. Lee, J. Huh, H. K. Yu, J. Choi, *Small* **2021**, *17*, 2102602.
[176] W. Wang, W. Wang, Y. Meng, Q. Quan, Z. Lai, D. Li, P. Xie, S. Yip, X. Kang, X. Bu, D. Chen, C. Liu, J. C. Ho, *ACS Nano* **2022**, *16*, 11036.
[177] H.-Y. Lee, G.-Z. Lu, J.-L. Shen, H.-Y. Lin, Y.-F. Chen, *J. Mater. Chem. C* **2022**, *10*, 16370.

[178] S. Cambré, M. Liu, D. Levshov, K. Otsuka, S. Maruyama, R. Xiang, *Small* **2021**, *17*, 2102585.
[179] X. Wang, C. J. Summers, Z. L. Wang, *Nano Lett.* **2004**, *4*, 423.
[180] X. Jiang, M. Yuan, H. Liu, L. Liubang, D. Zuliang, *Mater. Lett.* **2016**, *176*, 52.
[181] Z. Li, C. Liu, X. Zhang, G. Ren, W. Han, W. Guo, *Small* **2019**, *15*, 1804692.
[182] Y. Zheng, W. Wang, Y. Li, J. Lan, Y. Xia, Z. Yang, X. He, G. Li, *ACS Appl. Mater. Interfaces* **2019**, *11*, 13589.
[183] C. Zhang, J. Chen, S. Wang, L. Kong, S. W. Lewis, X. Yang, A. L. Rogach, G. Jia, *Adv. Mater.* **2020**, *32*, 2002736.
[184] K. Lefatshe, P. Dube, D. Sebuso, M. Madhuku, C. Muiva, *Ceram. Int.* **2021**, *47*, 7407.
[185] S. You, L. Zhang, Q. Yang, *Nano Res.* **2021**, *14*, 3386.
[186] H. Zhang, D. Lin, W. Liu, Y. Wang, Z. Li, D. Jin, J. Wang, X. Zhang, L. Huang, S. Wang, C. Xu, Y. Kan, L. Xie, *Adv. Mater. Interfaces* **2022**, *9*, 2200194.
[187] J. Xie, L. Wu, M. Cao, Q. Zhong, Y. Zeng, C. Ni, Q. Qian, X. Zhang, H. Huang, *Adv. Mater. Technol.* **2022**, *7*, 2200131.
[188] S. Lin, S. Li, H. Huang, H. Yu, Y. Zhang, *Small* **2022**, *18*, 2106420.
[189] Y. Cao, P. Qu, C. Wang, J. Zhou, M. Li, X. Yu, X. Yu, J. Pang, W. Zhou, H. Liu, G. Cuniberti, *Adv. Opt. Mater.* **2022**, *10*, 2200816.
[190] P. Avouris, M. Freitag, V. Perebeinos, *Nat. Photonics* **2008**, *2*, 341.
[191] M. Rivera, R. Velázquez, A. Aldalbahi, A. F. Zhou, P. Feng, *Sci. Rep.* **2017**, *7*, 42973.
[192] W. Xu, Y. Lu, W. Lei, F. Sui, R. Ma, R. Qi, R. Huang, *Micromachines* **2021**, *13*, 11.
[193] B. Kim, N. Park, J. Kim, *Nat. Commun.* **2022**, *13*, 3237.
[194] S. Mohammadnejad, S. Ahadzadeh, M. N. Rezaie, *Curr. Appl. Phys.* **2021**, *29*, 138.
[195] M. G. Burdanova, R. J. Kashtiban, Y. Zheng, R. Xiang, S. Chiashi, J. M. Woolley, M. Staniforth, E. Sakamoto-Rablah, X. Xie, M. Broome, J. Sloan, A. Anisimov, E. I. Kauppinen, S. Maruyama, J. Lloyd-Hughes, *Nano Lett.* **2020**, *20*, 3560.
[196] Z.-K. Tang, B. Wen, M. Chen, L.-M. Liu, *Adv. Theory Simul.* **2018**, *1*, 1800082.
[197] H.-H. Wu, Q. Meng, H. Huang, C. T. Liu, X.-L. Wang, *Phys. Chem. Chem. Phys.* **2018**, *20*, 3608.
[198] W. Huang, Y. Zhang, Q. You, P. Huang, Y. Wang, Z. N. Huang, Y. Ge, L. Wu, Z. Dong, X. Dai, Y. Xiang, J. Li, X. Zhang, H. Zhang, *Small* **2019**, *15*, 1900902.
[199] M. Zwawi, A. Attar, A. F. Al-Hossainy, M. H. Abdel-Aziz, M. S. Zoromba, *Chem. Pap.* **2021**, *75*, 6575.
[200] M. M. Mburu, K. Lu, N. L. Prine, A. Au-Duong, W. Chiang, X. Gu, Y. Chiu, *Adv. Mater. Technol.* **2022**, *7*, 2101506.
[201] P. Chithaiah, S. Ghosh, A. Idelevich, L. Rovinsky, T. Livneh, A. Zak, *ACS Nano* **2020**, *14*, 3004.
[202] S. W. Arafat, Z. K. Heiba, M. M. S. Sanad, H. Elshimy, H. S. AlSalem, A. M. Alenad, T. A. Taha, *Opt. Mater.* **2022**, *129*, 112561.
[203] X. Li, M. Rui, J. Song, Z. Shen, H. Zeng, *Adv. Funct. Mater.* **2015**, *25*, 4929.
[204] Q. Liu, H. Tian, J. Li, A. Hu, X. He, M. Sui, X. Guo, *Adv. Opt. Mater.* **2019**, *7*, 1900455.
[205] H. Tetsuka, A. Nagoya, T. Fukusumi, T. Matsui, *Adv. Mater.* **2016**, *28*, 4632.
[206] B. Pradhan, S. Das, J. Li, F. Chowdhury, J. Cherusseri, D. Pandey, D. Dev, A. Krishnaprasad, E. Barrios, A. Towers, A. Gesquiere, L. Tetard, T. Roy, J. Thomas, *Sci. Adv.* **2020**, *6*, eaay5225.
[207] T. Yuan, T. Meng, P. He, Y. Shi, Y. Li, X. Li, L. Fan, S. Yang, *J. Mater. Chem. C* **2019**, *7*, 6820.
[208] M. Tan, M. Li, W. Pan, X. Feng, Y. He, J. Liu, F. Dong, H. Wei, B. Yang, *Light: Sci. Appl.* **2022**, *11*, 304.
[209] Y. Li, H. Shu, S. Wang, J. Wang, *J. Phys. Chem. C* **2015**, *119*, 4983.
[210] C. Berger, Z. Song, X. Li, X. Wu, N. Brown, C. Naud, D. Mayou, T. Li, J. Hass, A. N. Marchenkov, E. H. Conrad, P. N. First, W. A. De Heer, *Science* **2006**, *312*, 1191.
[211] M. Fu, F. Ehrat, Y. Wang, K. Z. Milowska, C. Reckmeier, A. L. Rogach, J. K. Stolarczyk, A. S. Urban, J. Feldmann, *Nano Lett.* **2015**, *15*, 6030.
[212] J. Chen, D. Jia, J. Qiu, R. Zhuang, Y. Hua, X. Zhang, *Nano Energy* **2022**, *96*, 107140.
[213] X. Jing, D. Zhou, R. Sun, Y. Zhang, Y. Li, X. Li, Q. Li, H. Song, B. Liu, *Adv. Funct. Mater.* **2021**, *31*, 2100930.
[214] S. Kadian, S. K. Sethi, G. Manik, *Mater. Chem. Front.* **2021**, *5*, 627.
[215] A. R. Kirmani, M. Woodhouse, J. M. Luther, *ACS Energy Lett.* **2022**, *7*, 1255.
[216] J. S. Benas, F. C. Liang, W. C. Chen, C. W. Hung, J. Y. Chen, Y. Zhou, S. T. Han, R. Borsali, C. C. Kuo, *Chem. Eng. J.* **2022**, *431*, 133701.
[217] X. Tang, M. M. Ackerman, M. Chen, P. Guyot-Sionnest, *Nat. Photonics* **2019**, *13*, 277.
[218] Y. Dong, M. Chen, W. K. Yiu, Q. Zhu, G. Zhou, S. v. Kershaw, N. Ke, C. P. Wong, A. L. Rogach, N. Zhao, *Adv. Sci.* **2020**, *7*, 2000068.
[219] D. Chen, Y. Liu, B. Xia, L. Chen, Y. Yang, G. Yang, J. Liu, S. Lu, C. Ge, P. Liu, J. Yang, G. Liang, X. Lan, X. Zeng, L. Li, J. Zhang, Z. Xiao, L. Gao, J. Tang, *Adv. Funct. Mater.* **2023**, *33*, 2210158.
[220] J. Arumugam, A. George, A. D. Raj, A. A. Irudayaraj, R. L. Josephine, S. J. Sundaram, A. M. Al-Mohaimeed, W. A. Al-onazi, M. S. Elshikh, K. Kaviyarasu, *J. Alloys Compd.* **2021**, *863*, 158681.
[221] Y. Zhang, W. Shen, S. Wu, W. Tang, Y. Shu, K. Ma, B. Zhang, P. Zhou, S. Wang, *ACS Nano* **2022**, *16*, 19187.
[222] X. Chen, H. Yang, G. Liu, F. Gao, M. Dai, Y. Hu, H. Chen, W. Cao, P. Hu, W. Hu, *Adv. Funct. Mater.* **2018**, *28*, 1705153.
[223] E. Georgitzikis, P. E. Malinowski, J. Maes, A. Hadipour, Z. Hens, P. Heremans, D. Cheyns, *Adv. Funct. Mater.* **2018**, *28*, 1804502.
[224] C. Livache, B. Martinez, N. Goubet, C. Gréboval, J. Qu, A. Chu, S. Royer, S. Ithurria, M. G. Silly, B. Dubertret, E. Lhuillier, *Nat. Commun.* **2019**, *10*, 2125.
[225] W. Tian, H. Sun, L. Chen, P. Wangyang, X. Chen, J. Xiong, L. Li, *InfoMat* **2019**, *1*, 140.
[226] Z. Li, Z. Li, Z. Shi, X. Fang, *Adv. Funct. Mater.* **2020**, *30*, 2002634.
[227] Y. Tchoe, M. S. Song, H. Kim, H. Baek, J. Y. Park, H. Oh, K. Lee, K. Chung, J. K. Hyun, G. C. Yi, *Nano Energy* **2020**, *76*, 104955.
[228] S. Praveen, S. Veeralingam, S. Badhulika, *Adv. Mater. Interfaces* **2021**, *8*, 2100373.
[229] A. Rogalski, P. Martyniuk, M. Kopytko, *Prog. Quantum Electron.* **2019**, *68*, 100228.
[230] H. Seung, C. Choi, D. C. Kim, J. S. Kim, J. H. Kim, J. Kim, S. I. Park, J. A. Lim, J. Yang, M. K. Choi, T. Hyeon, D.-H. Kim, *Sci. Adv.* **2022**, *8*, eabq3101.
[231] J. Liu, P. Liu, D. Chen, T. Shi, X. Qu, L. Chen, T. Wu, J. Ke, K. Xiong, M. Li, H. Song, W. Wei, J. Cao, J. Zhang, L. Gao, J. Tang, *Nat. Electron.* **2022**, *5*, 443.
[232] H. Wu, H. Si, Z. Zhang, Z. Kang, P. Wu, L. Zhou, S. Zhang, Z. Zhang, Q. Liao, Y. Zhang, *Adv. Sci.* **2018**, *5*, 1801219.
[233] S. Pak, Y. Cho, J. Hong, J. Lee, S. Lee, B. Hou, G.-H. An, Y.-W. Lee, J. E. Jang, H. Im, S. M. Morris, J. I. Sohn, S. Cha, J. M. Kim, *ACS Appl. Mater. Interfaces* **2018**, *10*, 38264.
[234] J. L. Liu, H. Wang, X. Li, H. Chen, Z. K. Zhang, W. W. Pan, G. Q. Luo, C. L. Yuan, Y. L. Ren, W. Lei, *J. Alloys Compd.* **2019**, *798*, 656.
[235] M. Peng, R. Xie, Z. Wang, P. Wang, F. Wang, H. Ge, Y. Wang, F. Zhong, P. Wu, J. Ye, Q. Li, L. Zhang, X. Ge, Y. Ye, Y. Lei, W. Jiang, Z. Hu, F. Wu, X. Zhou, J. Miao, J. Wang, H. Yan, C. Shan, J. Dai, C. Chen, X. Chen, W. Lu, W. Hu, *Sci. Adv.* **2021**, *7*, eabf7358.
[236] H.-Y. Lan, Y.-H. Hsieh, Z.-Y. Chiao, D. Jariwala, M.-H. Shih, T.-J. Yen, O. Hess, Y.-J. Lu, *Nano Lett.* **2021**, *21*, 3083.
[237] L. Zheng, W. Zhou, Z. Ning, G. Wang, X. Cheng, W. Hu, W. Zhou, Z. Liu, S. Yang, K. Xu, M. Luo, Y. Yu, *Adv. Opt. Mater.* **2018**, *6*, 1800985.

[238] T. Chen, C. Wang, G. Yang, Q. Lou, Q. Lin, S. Zhang, H. Zhou, *Adv. Mater. Technol.* **2023**, *8*, 2200679.
[239] M. Zhang, Z. Chi, G. Wang, Z. Fan, H. Wu, P. Yang, J. Yang, P. Yan, Z. Sun, *Adv. Mater.* **2022**, *34*, 2205679.
[240] R. Ferreira, M. Shaikh, S. K. Jakka, J. Deuermeier, P. Barquinha, S. Ghosh, E. Fortunato, R. Martins, S. Jana, *Nano Lett.* **2022**, *22*, 9020.
[241] G. Sun, R. Ling, Y. Cai, A. Wang, *J. Electron. Mater.* **2023**, *52*, 368.
[242] M. Ikram, S. Rasheed, A. M. Afzal, N. A. Shad, Y. Javed, A. Mohyuddin, T. Alomayri, M. M. Sajid, A. Almahri, D. Hussain, *J. Alloys Compd.* **2022**, *909*, 164753.
[243] Q. Xiao, X. Li, Z. Zhang, C. Hu, G. Dun, B. Sun, Y. Peng, Q. Wang, Z. Zheng, H. Zhang, *Adv. Electron. Mater.* **2020**, *6*, 2000240.
[244] J. Yang, W. Kang, Z. Liu, M. Pi, L. B. Luo, C. Li, H. Lin, Z. Luo, J. Du, M. Zhou, X. Tang, *J. Phys. Chem. Lett.* **2020**, *11*, 6880.
[245] Q. Xu, I. T. Cheong, L. Meng, J. G. C. Veinot, X. Wang, *ACS Nano* **2021**, *15*, 18429.
[246] H. Wang, P. Zhang, Z. Zang, *Appl. Phys. Lett.* **2020**, *116*, 162103.
[247] K. Shen, H. Xu, X. Li, J. Guo, S. Sathasivam, M. Wang, A. Ren, K. L. Choy, I. P. Parkin, Z. Guo, J. Wu, *Adv. Mater.* **2020**, *32*, 2000004.
[248] C. Bi, S. V. Kershaw, A. L. Rogach, J. Tian, *Adv. Funct. Mater.* **2019**, *29*, 1902446.
[249] K. Xu, X. Xiao, W. Zhou, X. Jiang, Q. Wei, H. Chen, Z. Deng, J. Huang, B. Chen, Z. Ning, *ACS Appl. Mater. Interfaces* **2020**, *12*, 15414.
[250] X. Huang, Y. Liu, G. Liu, K. Liu, X. Wei, M. Zhu, W. Wen, Z. Zhao, Y. Guo, Y. Liu, *Adv. Funct. Mater.* **2023**, *33*, 2208836.
[251] H.-S. Zhang, X.-M. Dong, Z.-C. Zhang, Z.-P. Zhang, C.-Y. Ban, Z. Zhou, C. Song, S.-Q. Yan, Q. Xin, J.-Q. Liu, Y.-X. Li, W. Huang, *Nat. Commun.* **2022**, *13*, 4996.
[252] Q.-B. Zhu, B. Li, D.-D. Yang, C. Liu, S. Feng, M.-L. Chen, Y. Sun, Y.-N. Tian, X. Su, X.-M. Wang, S. Qiu, Q.-W. Li, X.-M. Li, H.-B. Zeng, H.-M. Cheng, D.-M. Sun, *Nat. Commun.* **2021**, *12*, 1798.
[253] H. Tan, Z. Ni, W. Peng, S. Du, X. Liu, S. Zhao, W. Li, Z. Ye, M. Xu, Y. Xu, X. Pi, D. Yang, *Nano Energy* **2018**, *52*, 422.
[254] Y. Sun, Y. Ding, D. Xie, *Adv. Funct. Mater.* **2021**, *31*, 2105625.
[255] Y.-X. Hou, Y. Li, Z.-C. Zhang, J.-Q. Li, D.-H. Qi, X.-D. Chen, J.-J. Wang, B.-W. Yao, M.-X. Yu, T.-B. Lu, J. Zhang, *ACS Nano* **2021**, *15*, 1497.
[256] M. C. Sahu, S. Sahoo, S. K. Mallik, A. K. Jena, S. Sahoo, *Adv. Mater. Technol.* **2023**, *8*, 2201125.
[257] S. Seo, J. Lee, R. Lee, T. H. Kim, S. Park, S. Jung, H. Lee, M. Andreev, K. Lee, K. Jung, S. Oh, H. Lee, K. S. Kim, G. Y. Yeom, Y. Kim, J. Park, *Adv. Mater.* **2021**, *33*, 2102980.
[258] Y. Pei, Z. Li, B. Li, Y. Zhao, H. He, L. Yan, X. Li, J. Wang, Z. Zhao, Y. Sun, Z. Zhou, J. Zhao, R. Guo, J. Chen, X. Yan, *Adv. Funct. Mater.* **2022**, *32*, 2203454.
[259] M. M. Islam, A. Krishnaprasad, D. Dev, R. Martinez-Martinez, V. Okonkwo, B. Wu, S. S. Han, T.-S. Bae, H.-S. Chung, J. Touma, Y. Jung, T. Roy, *ACS Nano* **2022**, *16*, 10188.
[260] L. Li, Z. Lou, G. Shen, *Adv. Funct. Mater.* **2018**, *28*, 1705389.
[261] J. Du, H. Yu, B. Liu, M. Hong, Q. Liao, Z. Zhang, Y. Zhang, *Small Methods* **2021**, *5*, 2000919.
[262] F. Cao, W. Tian, M. Wang, H. Cao, L. Li, *Adv. Funct. Mater.* **2019**, *29*, 1901280.
[263] J. Zhang, T. Sun, S. Zeng, D. Hao, B. Yang, S. Dai, D. Liu, L. Xiong, C. Zhao, J. Huang, *Nano Energy* **2022**, *95*, 106987.
[264] R. Ding, Y. Lyu, Z. Wu, F. Guo, W. F. Io, S. Pang, Y. Zhao, J. Mao, M. Wong, J. Hao, *Adv. Mater.* **2021**, *33*, 2101263.
[265] M. Kataria, K. Yadav, G. Haider, Y. M. Liao, Y.-R. Liou, S.-Y. Cai, H. Lin, Y. H. Chen, C. R. Paul Inbaraj, K. P. Bera, H. M. Lee, Y.-T. Chen, W.-H. Wang, Y. F. Chen, *ACS Photonics* **2018**, *5*, 2336.
[266] M. Z. Nawaz, L. Xu, X. Zhou, J. Li, K. H. Shah, J. Wang, B. Wu, C. Wang, *ACS Appl. Mater. Interfaces* **2022**, *14*, 19659.
[267] A. Shultz, B. Liu, M. Gong, M. Alamri, M. Walsh, R. C. Schmitz, J. Z. Wu, *ACS Appl. Nano Mater.* **2022**, *5*, 16896.
[268] Z. Lai, Y. Meng, Q. Zhu, F. Wang, X. Bu, F. Li, W. Wang, C. Liu, F. Wang, J. C. Ho, *Small* **2021**, *17*, 2100442.
[269] H. Kim, S. Z. Uddin, D.-H. Lien, M. Yeh, N. S. Azar, S. Balendhran, T. Kim, N. Gupta, Y. Rho, C. P. Grigoropoulos, K. B. Crozier, A. Javey, *Nature* **2021**, *596*, 232.
[270] H.-J. Kim, H. Oh, T. Kim, D. Kim, M. Park, *ACS Appl. Nano Mater.* **2022**, *5*, 1308.

Jaehyun Kim is currently a postdoctoral scholar with the Department of Chemistry and Materials Research Center at the Northwestern University, IL, USA, under the supervision of Prof. Antonio Facchetti and Tobin J. Marks. His research focuses on developing high-performance nanomaterials-based optoelectronic devices, including thin-film transistors, sensors, and photodetectors. His current areas of research interest include flexible/wearable optoelectronics and photo/image sensor arrays based on multispectral semiconductors, such as quantum dots, organic, and metal–oxide for biomedical/imaging applications.

Junho Lee received Master degree in electrical & electronics engineering from Chung-Ang university, Seoul, Korea, with a thesis focused on stretchable tactile sensors with machine-learned neural network system. Afterward, he continued to study optoelectronics along with the same subject and is currently in the process of obtaining his Ph.D. degree as a candidate. His research interest includes stretchable, flexible electronics and tactile sensors such as strain, pressure, and tactile sensor. He is also interested in the development of nanostructures for photodetectors and thin film transistors for flexible and stretchable circuit.

Jong-Min Lee received a Bachelor's degree in physics from Chung-Ang University in Seoul, Korea, with a thesis focused on optics and semiconductor physics. He continued to study optoelectronics and is currently pursuing an integrated Master's and Ph.D. program. His research interests include heterojunction phototransistors, CMOS oxide transistors, and oxide neuromorphic circuits. He is also interested in developing photo-neuromorphic circuits and thin-film transistors.

Antonio Facchetti is a co-founder and currently the chief technology officer of Flexterra Corporation. He is also an adjunct professor at Northwestern University and a guest professor at Linkoping University. He has published more than 560 research articles, 15 book chapters, and holds more than 120 patents. He received the ACS Award for Creative Invention, the Giulio Natta Gold Medal of the Italian Chemical Society, the team IDTechEx Printed Electronics Europe Award, the corporate Flextech Award. He is a fellow of the European Academy of Sciences, National Academy of Inventors, MRS, AAAS, PMSE, Kavli, and RSC.

Tobin J. Marks is Ipatieff professor of chemistry and materials science and engineering at Northwestern University. He holds a B.S. from the University of Maryland and a Ph.D. from MIT. Awards: U.S. National Medal of Science, Spanish Asturias Prize, MRS Von Hippel Award, Dreyfus Prize in Chemical Sciences, NAS Award in Chemical Sciences, ACS Priestley Medal, and Technion Harvey Prize. Membership: U.S., European, German, Italian, and Indian Academies of Science, U.S. NAE and NAI, American Academy of Arts and Sciences; RSC, MRS, ACS Fellow.

Sung Kyu Park is the Professor of school of electrical and electronics engineering at Chung-Ang. University, Seoul, Korea. He received his Ph. D degree from The Pennsylvania State University, University Park, PA in 2007. He was employed at Korea Electronics Technology Institute (KETI) and Eastman Kodak Company, Rochester, NY. After twenty years at the KETI, Eastman Kodak Research Center, and Chung-Ang University, Prof. Park's research focuses on exploratory electronic materials and devices. His current areas of research interest include quantum dots, organic, metal-oxide, chalcogenide materials and their applications such as opto-electronic devices, display technologies, neuromorphic devices, and systems.